

Shortcomings of meta-GGA functionals when describing magnetism

Fabien Tran,¹ Guillaume Baudesson,^{1,2} Jesús Carrete,¹ Georg K. H. Madsen,¹ Peter Blaha,¹ Karlheinz Schwarz,¹ and David J. Singh³

¹*Institute of Materials Chemistry, Vienna University of Technology, Getreidemarkt 9/165-TC, A-1060 Vienna, Austria*

²*Univ Rennes, ENSCR, CNRS, ISCR (Institut des Sciences Chimiques de Rennes) - UMR 6226, F-35000 Rennes, France*

³*Department of Physics and Astronomy, University of Missouri, Columbia, Missouri 65211-7010, USA*

Several recent studies have shown that SCAN, a functional belonging to the meta-generalized gradient approximation (MGGA) family, leads to significantly overestimated magnetic moments in itinerant ferromagnetic metals. However, this behavior is not inherent to the MGGA level of approximation since TPSS, for instance, does not lead to such severe overestimations. In order to provide a broader view of the accuracy of MGGA functionals for magnetism, we extend the assessment to more functionals, but also to antiferromagnetic solids. The results show that to describe magnetism there is overall no real advantage in using a MGGA functional compared to GGAs. For both types of approximation, an improvement in ferromagnetic metals is necessarily accompanied by a deterioration (underestimation) in antiferromagnetic insulators, and vice-versa. We also provide some analysis in order to understand in more detail the relation between the mathematical form of the functionals and the results.

I. INTRODUCTION

The local density approximation¹ (LDA) and generalized gradient approximation^{2,3} (GGA) of density functional theory^{1,4} (DFT) usually provide a fair description of the magnetism in itinerant ferromagnetic (FM) 3d metals, albeit a slight overestimation of the magnetic moment can be obtained (see, e.g., Refs. 5–7). On the other hand, the LDA and GGA are inaccurate for antiferromagnetic (AFM) insulators, where the 3d electrons are more localized and the self-interaction error (SIE)⁸ present in LDA and GGA is more important. As a consequence, the atomic moment around the transition-metal atom in AFM systems is clearly underestimated.⁹

The exchange-correlation (xc) functionals of the meta-GGA (MGGA) level of approximation^{10,11} should in general be more accurate since they use an additional ingredient, the kinetic-energy density (KED), which makes possible to remove a portion of the SIE.¹² The strongly constrained and appropriately normed (SCAN) MGGA functional proposed recently by Sun *et al.*¹³ was constructed in such a way that it satisfies all the 17 known mathematical constraints that can be imposed on a MGGA functional, and was appropriately normed, i.e. made accurate, for particular systems. The SCAN functional has been shown to be accurate for both molecules and solids,^{13–16} including systems bound by noncovalent interactions provided that a dispersion term is added.^{17–19} On the other hand, it has been realized that SCAN leads to magnetic moments in bulk FM Fe, Co, and Ni that are by far too large.^{16,20–24} The overestimation of the magnetic moment with SCAN has also been observed in alloys^{25,26} and surface systems.²⁷

Nevertheless, this overestimation of magnetic moments is not inherent to the MGGA, since other MGGA functionals like TPSS,²⁸ revTPSS,²⁹ and TM³⁰ lead to values similar to PBE.^{20,23,31} Interestingly, Mejía-Rodríguez and Trickey²⁴ showed that SCAN-L, a deorbitalized ver-

sion of SCAN they proposed in Refs. 32 and 33, leads to a magnetic moment which is similar to PBE, while the results for the geometry and binding energy of molecules and solids stay close to the original SCAN.^{32–34}

Regarding the general performance of MGGA functionals for magnetism in solids, a few questions remain. For instance, not that many results for the atomic magnetic moment in AFM systems have been reported. Recent tests on various oxides have shown that SCAN underestimates the moment in some cases like MnO or Fe₂O₃, but overestimates it in MnO₂.^{35,36} In Refs. 37 and 38, the FM and AFM phases of VO₂ were studied with numerous functionals including TPSS, revTPSS, MGGA_MS0,³⁹ MGGA_MS2,⁴⁰ and SCAN. It was shown that the latter three functionals lead to moments that are larger than those predicted by TPSS and revTPSS, especially for the AFM phase. Comparisons with reference Monte-Carlo results for the AFM phase of VO₂ indicate that MGGA_MS0, MGGA_MS2, and SCAN should be more accurate.^{37,38} In Ref. 41, the high-*T_c* superconductor parent compound La₂CuO₄ were studied with TPSS, revTPSS, and SCAN, the latter giving a value of the moment of the Cu atom in good agreement with experiment, while a clear underestimation is obtained with TPSS and revTPSS. A recent study by Zhang *et al.* has shown that SCAN underestimates the atomic magnetic moment in MnO, FeO, CoO, and NiO.⁴² Finally, it has been reported that SCAN leads to a magnetic moment in AFM α -Mn that is much larger than with PBE.⁴³

Despite these results for FM and AFM systems, what is missing is a more systematic study of the relative performance of MGGA functionals for magnetism. In particular, besides SCAN and (rev)TPSS, not much is known about the performance of other MGGA functionals. It is also not fully clear to which extent an increase (e.g., with respect to PBE) of the moment in FM solids with a given MGGA necessarily translates into an increase for AFM solids. In the present work, a more systematic

comparison of MGGA functionals for magnetism is presented. FM and AFM systems are considered, as well as nonmagnetic (NM) ones. The latter may be wrongly described as magnetic with DFT methods.^{22,44} The search for a possible magnetic ground state for the supposedly NM systems is restricted to FM.

The paper is organized as follows. A description of the methods is given in Sec. II. In Sec. III, the results are presented and discussed, and Sec. V gives the summary of this work.

II. METHODS

Among the plethora of MGGA functionals that exist,⁴⁵ we selected a few representatives of various types; empirical vs. non-empirical, old standard vs. modern, general purpose vs. specialized for a particular property. These are the following: BR89,⁴⁶ TPSS,²⁸ revTPSS,²⁹ MGGA_MS2,⁴⁰ MVS,⁴⁷ SCAN,¹³ TM,³⁰ HLE17,⁴⁸ SCAN-L,^{32,33} and TASK.⁴⁹ Here, we just mention that HLE17 consists in a simple empirical rescaling of TPSS exchange and correlation, which are multiplied by 1.25 and 0.5, respectively, in order to achieve better results for the band gaps of solids and excitation energies of molecules.⁴⁸ The very recent TASK from Aschbrock and Kümmel,⁴⁹ which is an exchange functional that is combined with LDA correlation,⁵⁰ also provides accurate band gaps, but in contrast to HLE17 it was constructed in a nonempirical way without tuning parameters. All MGGA except SCAN-L and BR89 are *t*-MGGA since they depend on the Kohn-Sham (KS) KED $t_\sigma = (1/2) \sum_{i=1}^{N_\sigma} \nabla \psi_{i\sigma}^* \cdot \nabla \psi_{i\sigma}$ (σ is the spin index). SCAN-L is a deorbitalized version of SCAN. A *t*-MGGA is deorbitalized^{32,51,52} by replacing t_σ by an orbital-free (and thus necessarily approximate) expression that depends on ρ_σ , $\nabla \rho_\sigma$, and $\nabla^2 \rho_\sigma$, and is thereby turned into a $\nabla^2 \rho$ -MGGA, which is an explicit functional of the electron density. The BR89 exchange functional of Becke and Roussel, which was proposed as an accurate approximation to the Hartree-Fock exchange energy,⁴⁶ depends on both t_σ and $\nabla^2 \rho_\sigma$. BR89, which is combined in this work with LDA correlation,⁵⁰ is tested since it differs radically from the other MGGA in terms of construction. Therefore, it may be interesting to see the results obtained with such a functional.

For comparison, the results obtained with the $(t_\sigma, \nabla^2 \rho_\sigma)$ -dependent modified Becke-Johnson (mB-JLDA) potential,⁵³ LDA,⁵⁰ and the two GGAs PBE⁵⁴ and HLE16⁵⁵ are also shown. HLE16 was constructed specifically for band gaps in a similar way as HLE17, by rescaling the exchange and correlation parts (with 1.25 and 0.5, respectively) of the highly parameterized GGA HCTH/407.⁵⁶ The mBJLDA potential was also proposed specifically for band gap calculations, for which it is currently the most accurate semilocal method.^{57–59}

The calculations were performed with the all-electron WIEN2k code,^{60,61} which is based on the linearized aug-

mented plane-wave (LAPW) method.^{62–64} Among the functionals, HLE17 and TASK were taken from the library of exchange-correlation functionals Libxc.^{65,66} The MGGA functionals are not implemented self-consistently in WIEN2k, i.e., only the total energy can be calculated. Nevertheless, it is still possible to calculate the magnetic moment without the corresponding MGGA potential by using only the total energy. The fixed spin-moment (FSM) method⁶⁷ (used for a part of the calculations presented in Refs. 22–24) can be used to calculate the magnetic moment of FM systems. The FSM method can not be applied to AFM systems, nevertheless, in the same spirit, the atomic moment can to some extent be constrained to have a chosen value. This can be done by adding and subtracting a constant shift C to the spin-up and spin-down xc potentials (of a given GGA functional), respectively, inside the LAPW sphere surrounding a transition-metal atom:

$$v_{xc+\text{shift},\sigma}^{\text{GGA}}(\mathbf{r}) = v_{xc,\sigma}^{\text{GGA}}(\mathbf{r}) + \sigma C, \quad (1)$$

where $\sigma = 1$ (-1) for spin-up (spin-down) electrons. Supposing that for an atom the spin-up electrons are majority, a negative (positive) C should increase (decrease) the magnitude of the spin magnetic moment. Obviously, in order to keep the AFM state, shifts C of the same magnitude, but with opposite signs have to be applied to the transition-metal atoms with opposite sign of the magnetic moment. As with the FSM method for FM solids, the variational principle is used: for a given MGGA functional, the spin atomic moment is the one obtained at the value of C which leads to the lowest total energy.

The fact that MGGA functionals are applied non-self-consistently also means that for both the FSM and C -shift methods the xc potential corresponding to another functional, typically a GGA, has to be used to generate the orbitals $\psi_{i\sigma}$. In a recent study⁶⁸ we showed that the non-self-consistent calculation of band gaps with MGGA can be done accurately, provided that an appropriate GGA potential to generate the orbitals is chosen. The criterion to choose the potential was based on the variational principle; among a plethora of GGA potentials, the one that is chosen is the one yielding orbitals that lead to the lowest total MGGA energy. As expected, these optimal orbitals also lead to band gaps that are the closest to the true MGGA band gaps obtained self-consistently from another code. That just means that in order to reproduce the true (i.e., self-consistent) MGGA results, one should use GGA orbitals which, according to the variational principle, are the closest to the MGGA orbitals. In the present study, the GGA orbitals that are used are those recommended in Ref. 68, namely RPBE⁶⁹ (for TPSS, revTPSS, MGGA_MS2, SCAN, TM, and SCAN-L), EV93PW91^{3,70} (for MVS), and mRPBE⁶⁸ (for HLE17). For TASK and BR89, not considered in Ref. 68, the orbitals generated by the GGAs RPBE and PBE potentials (among all GGA potentials that we have tried, those listed in Ref. 68), respectively, lead to the lowest total energy. Therefore, in the present study the

TASK and BR89 functionals have been calculated with the RPBE and PBE orbitals, respectively.

In order to validate our procedure, the magnetic moments obtained self-consistently with the VASP⁷¹ and GPAW codes,^{72,73} both are based on the projector augmented wave (PAW) method,⁷⁴ will be compared to our results for a few test cases.

Another technical point concerns the definition of the atomic magnetic moment in AFM solids. Since there is no unique way to define an atom in a molecule or solid, the region of integration around an atom to calculate the atomic moment can to some extent be chosen arbitrarily. In solid-state physics, basis sets like LAPW⁶² or PAW⁷⁴ use spheres surrounding the atoms, which are commonly used to define the atoms and to calculate the corresponding magnetic moment. As shown in Sec. III, different radii may lead to quite different values of the atomic moment. A way to define the region of integration independently of the basis set is to use the quantum theory of atoms in molecules (QTAIM) of Bader.^{75,76} In QTAIM, the volume of an atom (usually called basin) is delimited by a surface with zero flux in the gradient of the electron density. The atomic moments of the AFM solids presented in Sec. III were obtained using the QTAIM as implemented in the Critic2 code.^{77,78} There is probably only very few works comparing the value of the atomic moment obtained from different definitions of the atom, therefore such a comparison will also be discussed in Sec. III.

The solids that are considered for the present study are listed in Table I along with their experimental geometry^{79,80} used for the calculations. The set is divided into five NM, seven FM, and nine AFM solids. We mention that for Fe, Fu and Singh^{22,23} considered the effect of the lattice constant on the magnetic moment. It can be non-negligible if a functional leads to an inaccurate lattice constant that is far from the experimental one. For instance, compared to the value obtained at the experimental lattice constant, the LDA magnetic moment is smaller by $\sim 0.2 \mu_B$ when it is calculated at the corresponding LDA lattice constant. For the present work, no optimization of the geometry was done, i.e., the calculations were performed at the same (experimental) geometry with all functionals. The reasons are the following. First, the effect of geometry and functional on the magnetic moment would be entangled, which would lead to a more complicated analysis and discussion of the results. Second, some of the tested functionals lead to extremely poor lattice constants (see Sec. IV), so that it would not make sense to calculate a property at such inaccurate geometry.

TABLE I. Experimental^{79,80} lattice constants (in Å) and angles (in degrees) of the unit cell for the solids considered in this work. When necessary, the positions of atoms (in fractional coordinates) are also indicated. The space group number is indicated in parenthesis. For the AFM solids, the AFM order leads to a lowering of the symmetry (second indicated space group).

Solid	<i>a</i>	<i>b</i>	<i>c</i>	α	β	γ
NM						
Sc (194)	3.309	3.309	5.273	90	90	120
V (229)	3.028	3.028	3.028	90	90	90
Y (194)	3.652	3.652	5.747	90	90	120
Pd (225)	3.881	3.881	3.881	90	90	90
Pt (225)	3.916	3.916	3.916	90	90	90
FM						
Fe (229)	2.867	2.867	2.867	90	90	90
Co (194)	2.507	2.507	4.070	90	90	120
Ni (225)	3.523	3.523	3.523	90	90	90
FeCo (221)	2.857	2.857	2.857	90	90	90
ZrZn ₂ (227)	7.396	7.396	7.396	90	90	90
Zr(1/8,1/8,1/8), Zn(1/2,0,0)						
YFe ₂ (227)	7.363	7.363	7.363	90	90	90
Y(1/8,1/8,1/8), Fe(1/2,0,0)						
Ni ₃ Al (221)	3.568	3.568	3.568	90	90	90
Ni(1/2,1/2,0), Al(0,0,0)						
AFM						
Cr ₂ O ₃ (167,146)	4.953	4.953	13.588	90	90	120
Cr(0,0,0.3475), O(0.3058,0,1/4)						
Fe ₂ O ₃ (167,146)	5.035	5.035	13.747	90	90	120
Fe(0,0,0.35534), O(0.3056,0,1/4)						
MnO (225,166)	4.445	4.445	4.445	90	90	90
FeO (225,166)	4.334	4.334	4.334	90	90	90
CoO (225,166)	4.254	4.254	4.254	90	90	90
NiO (225,166)	4.171	4.171	4.171	90	90	90
CuO (15,14)	4.684	3.423	5.129	90	99.54	90
Cu(1/4,1/4,0), O(0,0.4184,1/4)						
CrSb (194,164)	4.122	4.122	5.464	90	90	120
CrSb ₂ (58,14)	6.028	6.874	3.272	90	90	90
Cr(0,0,0), Sb(0.1835,0.3165,0.32)						

III. RESULTS

A. Choice of orbitals and atomic region

Before discussing the relative performance of the functionals, we show in Table II some results for MnO, FeO, CoO, and NiO in order to illustrate the influence of self-consistency and choice of integration region (i.e., definition of the atom) on the spin atomic magnetic moment μ_S . As mentioned in Sec. II and discussed in more de-

TABLE II. Spin atomic magnetic moment μ_S (in μ_B) of AFM MnO, FeO, CoO, and NiO. The results in the first three columns were obtained with WIEN2k using different atomic sphere sizes (their radii, in bohr, are indicated) for calculating μ_S . The results in the last three columns were obtained with three different codes and using the Bader volume for calculating μ_S . The WIEN2k results for the MGGA were obtained with the C -shift method [Eq. (1)] and using either the RPBE or PBE (results in parenthesis) orbitals. All VASP and GPAW results were obtained self-consistently. The calculations were done at the geometry specified in Table I.

	WIEN2k			Bader volume		
	Small sphere	Medium sphere	Large sphere	WIEN2k	VASP	GPAW
MnO						
Sphere radius	2.05	2.25	2.45			
PBE	4.19	4.31	4.38	4.39	4.38	4.37
TPSS	4.21	4.33	4.40	4.41 (4.42)	4.40	4.40
SCAN	4.32	4.44	4.51	4.53 (4.53)	4.50	4.49
FeO						
Sphere radius	2.00	2.20	2.40			
PBE	3.39	3.45	3.48	3.48	3.46	3.48
TPSS	3.43	3.49	3.53	3.52 (3.52)	3.49	3.51
SCAN	3.53	3.59	3.63	3.62 (3.62)	3.59	3.60
CoO						
Sphere radius	1.95	2.15	2.35			
PBE	2.42	2.45	2.45	2.45	2.43	2.45
TPSS	2.45	2.50	2.51	2.50 (2.39)	2.48	2.51
SCAN	2.55	2.59	2.61	2.60 (2.42)	2.59	2.61
NiO						
Sphere radius	1.90	2.10	2.30			
PBE	1.38	1.38	1.37	1.37	1.32	1.36
TPSS	1.47	1.47	1.46	1.46 (1.46)	1.42	1.45
SCAN	1.62	1.62	1.61	1.60 (1.60)	1.59	1.60

tail in Ref. 68, the GGA RPBE potential is the optimal one for the MGGA TPSS and SCAN. The importance of using the orbitals generated by the RPBE potential is visible in the case of CoO; compared to using the PBE orbitals (the usual default choice) μ_S is larger by about 0.1 and 0.2 μ_B for TPSS and SCAN, respectively. Such differences are not negligible, and in fact we can also see that using the RPBE orbitals brings the WIEN2k results into agreement with those obtained self-consistently with VASP and GPAW codes. We just note that for NiO there is a discernible discrepancy between VASP and the two other codes. After looking into this issue, we came to the conclusion that the problem may be due to VASP projectors that are unadapted for the particular case of NiO. For MnO, FeO, and NiO, using either PBE or RPBE orbitals does not matter at all. Indeed, we found that in the case of CoO the optimal choice of GGA orbitals (as listed in Sec. II) is critical to avoid values of μ_S that are too small by 0.1–0.2 μ_B as would be obtained with the PBE orbitals. The other cases where using the optimal orbitals (instead of the standard PBE) is also impor-

tant concern a few of the AFM and FM solids when the MGGA HLE17 is used, for which the optimal potential is mRPBE.

From the results in Table II, the other main observation is that the atomic volume inside which the atomic moment μ_S is calculated may have some influence as well. WIEN2k calculations were done with three different radii for the atomic sphere, which were chosen to lie within a reasonable range from a physical point of view, in particular not too small in order to avoid core leakage. The value of μ_S calculated from within the sphere varies the most for MnO; from the smallest sphere (2.05 bohr) to the largest (2.45 bohr) μ_S increases by about 0.2 μ_B , which is rather significant. On the other hand, there is no change in μ_S for NiO (since Ni has the largest nuclear charge Z and therefore the most localized $3d$ electrons), but of course reducing the sphere size further would at some point lead to a decrease of the magnetic moment. For FeO and CoO, the variation of μ_S is intermediate between MnO and NiO. The other important point to note is that in all cases the magnetic moment obtained with

the largest sphere agrees with the one obtained using the Bader volume.

Since the Bader volume is uniquely defined and the corresponding μ_S agrees with the value obtained with the largest LAPW atomic sphere, using it as the atomic region to calculate μ_S can be considered as a pretty sound choice. Therefore, the comparison of the functionals for the atomic magnetic moment in AFM solids will be based on the values obtained with the Bader volume.

B. Comparison of functionals

1. Ferromagnetic solids

We start the discussion on the comparison of the functionals with the FM solids. The results for the spin magnetic moment μ_S (per formula unit) are shown in Table III. It is known that the GGAs (and sometimes also the LDA) slightly overestimate the magnitude of μ_S in itinerant metals like Fe, Co, or Ni.^{5,6} For these systems, the overestimation with LDA and the standard GGA PBE is in the range 0.05–0.2 μ_B . The other GGA considered in this work, HLE16, leads to unpredictable results, since it yields a moment that is much larger (by 0.5 μ_B) than the one predicted by PBE for Fe, but to identical values for Ni, while the increase is 0.1 μ_B for Co. However, such behavior with HLE16 is not that surprising since, as shown in Ref. 57 and discussed in Sec. IV, it has a strong enhancement factor that leads to an xc potential with very large oscillations and therefore possibly unexpected results. The results obtained for the compounds show that LDA and PBE are accurate for FeCo, but overestimate μ_S for YFe₂ and significantly for ZrZn₂ and Ni₃Al. However, for the latter two systems spin fluctuations, which require a treatment beyond standard DFT, are supposed to significantly reduce the measured moment (see discussion in Ref. 91 for ZrZn₂ and in Refs. 92 and 93 for Ni₃Al). The results with HLE16 are again disparate; compared to PBE, μ_S is increased for FeCo and ZrZn₂, but reduced for YFe₂ and Ni₃Al. HLE16 leads to the best agreement with experiment for YFe₂, but to the worst for ZrZn₂.

Turning to the results obtained with the MGGA methods, we mention again that several studies have already reported that SCAN, which is highly successful in solid-state physics for total-energy calculations,^{15–17,19,94,95} clearly overestimates the magnetic moment in itinerant metals.^{16,20–24} Those studies considered mostly Fe, Co, and Ni which were considered. For the intermetallic ferromagnets considered here, the overestimation of μ_S with SCAN is also substantial. In fact, among all xc methods SCAN leads to one of the largest overestimations except for Fe and ZrZn₂. This makes SCAN an inaccurate functional for itinerant metals in general. The deorbitalized SCAN-L leads to (much) smaller value of μ_S compared to its parent functional, confirming the results from Ref. 24. Interestingly, among all methods SCAN-L leads to one

of the smallest magnetic moments for Fe. Thus one may suppose that the orbital dependence in SCAN, which is thought to be crucial for reducing the SIE, is at the same time problematic for itinerant systems.

Among the other MGGA, TPSS, revTPSS, TM, and BR89 lead on average to the smallest overestimations of the magnetic moment and to values that are only slightly larger (usually by less than 0.1 μ_B) than PBE. Note that, for ZrZn₂, TPSS and revTPSS give $\mu_S = 0.82 - 0.83 \mu_B$, which is smaller than 0.90 μ_B obtained with PBE. Concerning the other MGGA functionals, very large overestimations of the magnetic moment are obtained with MGGA_MS2 (YFe₂ and Ni₃Al), MVS (Fe, Co, Ni, and FeCo), HLE17 (ZrZn₂), and TASK (for all systems except YFe₂). On the other hand, HLE17 leads to a moment of 0.66 μ_B for Ni₃Al, which is smaller than the PBE value of 0.77 μ_B . Thus, HLE17 behaves in an erratic way just like HLE16 does. The mBJLDA potential clearly overestimates μ_S in all cases, but never leads to one of the most extreme values.

In summary, all functionals lead to overestimations of the magnetic moment, at least if the effects due to spin fluctuations are ignored. LDA, the GGA PBE, and the MGGA TPSS, revTPSS, TM, SCAN-L, and BR89 lead to the smallest deviations with respect to experiment, while TASK, SCAN, and MVS give the largest overestimations. The results obtained with the GGA HLE16 and MGGA HLE17 are erratic. In passing, we note that hybrid functionals also lead to magnetic moments in metals that are greatly overestimated, as shown in Refs. 20, 96–102 for the screened HSE06.^{103,104} The same conclusion applies to the GLLB-SC potential¹⁰⁵ (see Ref. 101 for results). Furthermore, we would like to provide two additional informations related to SCAN-L: (a) Among the other orbital-free KED used in Refs. 32 and 34 for deorbitalizing SCAN, we also tested GEA2L; it gives magnetic moments that are quasi-identical to SCAN-L. (b) A deorbitalization of TASK leads to a reduction of the magnetic moment that is roughly similar to SCAN-L. As discussed later in Sec. IV, this is due to a particular feature in the analytical forms of the SCAN and TASK functionals and differences between the iso-orbital indicator α and its deorbitalized version α_L .

Table IV shows the results obtained for the magnetic energy, defined as the difference

$$\Delta E_{\text{tot}} = E_{\text{tot}}^{\text{FM}} - E_{\text{tot}}^{\text{NM}} \quad (2)$$

between the total energies of the FM and NM (i.e., spin-unpolarized) states of the system. A negative value indicates that the FM state is more stable than the NM state, which is the case here for all solids and functionals. Note that no results are shown for mBJLDA, since it is only a potential with no corresponding xc energy functional.^{106,107} Considering all functionals except HLE16 and HLE17, there is a clear correlation between the magnetic moment and magnetic energy; the functionals leading to the largest values of μ_S (TASK, SCAN, and MVS) also lead to the largest values of ΔE_{tot} . This

TABLE III. Spin magnetic moment μ_S (in μ_B per formula unit) of FM solids. The experimental values for Fe, Co, and Ni are also spin magnetic moments. The results in parenthesis for FeCo are the atomic moments (defined according to the Bader volume) on Fe and Co. The results for the MGGA functionals were obtained with the FSM method. The calculations were done at the geometry specified in Table I. The largest discrepancies with respect to experiment are underlined.

Method	Fe	Co	Ni	FeCo	YFe ₂	ZrZn ₂	Ni ₃ Al
LDA	2.20	1.59	0.62	4.51(2.76,1.75)	3.20	<u>0.67</u>	<u>0.71</u>
PBE	2.22	1.62	0.64	4.55(2.81,1.75)	3.38	<u>0.90</u>	<u>0.77</u>
HLE16	<u>2.74</u>	1.73	0.64	4.77(3.06,1.71)	2.91	<u>1.72</u>	<u>0.57</u>
mBJLDA	2.51	1.69	0.73	4.60(2.87,1.73)	3.60	<u>0.95</u>	<u>0.85</u>
TPSS	2.23	1.65	0.66	4.63(2.86,1.77)	3.66	<u>0.82</u>	<u>0.80</u>
revTPSS	2.29	1.67	0.68	4.67(2.89,1.79)	3.71	<u>0.83</u>	<u>0.83</u>
MGGA_MS2	2.30	1.74	0.73	4.80(2.96,1.84)	<u>3.81</u>	0.98	0.95
MVS	<u>2.71</u>	<u>1.80</u>	<u>0.76</u>	<u>4.88</u> (3.01,1.87)	3.69	1.04	<u>0.84</u>
SCAN	2.63	<u>1.79</u>	<u>0.76</u>	<u>4.86</u> (2.99,1.87)	<u>3.88</u>	<u>1.08</u>	<u>0.95</u>
TM	2.25	1.68	0.69	4.69(2.89,1.79)	3.67	<u>0.88</u>	<u>0.85</u>
HLE17	2.67	1.72	0.65	4.74(3.02,1.71)	3.60	<u>1.27</u>	<u>0.66</u>
TASK	<u>2.75</u>	<u>1.83</u>	<u>0.76</u>	<u>4.91</u> (3.02,1.89)	3.45	<u>1.37</u>	<u>0.89</u>
SCAN-L	2.13	1.65	0.68	4.62(2.85,1.77)	3.26	<u>1.03</u>	<u>0.84</u>
BR89	2.45	1.67	0.66	4.64(2.86,1.78)	3.74	<u>0.83</u>	<u>0.76</u>
Expt.	1.98, ^a 2.05, ^b 2.08 ^c	1.52, ^c 1.58, ^{b,d} 1.55-1.62 ^a	0.52, ^c 0.55 ^{b,e}	4.54 ^f	2.90 ^g	0.17 ^h	0.23 ⁱ

^a Ref. 81.

^b Ref. 82.

^c Ref. 83.

^d Ref. 84.

^e Ref. 85.

^f Ref. 86.

^g Ref. 87.

^h Refs. 88 and 89.

ⁱ Ref. 90.

TABLE IV. Magnetic energy $-\Delta E_{\text{tot}}$ (in meV per formula unit) of FM solids. The results for the MGGA functionals were obtained with the FSM method. The calculations were done at the geometry specified in Table I.

Method	Fe	Co	Ni	FeCo	YFe ₂	ZrZn ₂	Ni ₃ Al
LDA	446	200	51	987	469	8	9
PBE	565	256	62	1260	658	47	22
HLE16	2050	909	132	3534	4186	247	24
TPSS	640	290	71	1447	762	25	34
revTPSS	678	315	77	1542	829	25	38
MGGA_MS2	868	414	109	2074	1123	68	87
MVS	1417	685	129	2734	2036	97	50
SCAN	1061	557	132	2503	1434	137	82
TM	711	333	84	1632	889	46	48
HLE17	1491	647	107	2773	2205	149	31
TASK	1630	789	148	3314	2620	225	67
SCAN-L	623	273	74	1473	694	109	44
BR89	771	372	79	1663	928	39	30

trend was observed in Refs. 22–24 and is connected with the magnetic susceptibility. However, HLE16 and HLE17

do not really follow this trend. For instance, for Ni and YFe₂ HLE16 gives the smallest magnetic moment, but the largest value for ΔE_{tot} . Similar observations can be made with HLE17.

Figure 1 shows ΔE_{tot} as a function of μ_S in the cases of Fe, Ni, ZrZn₂, and Ni₃Al. As discussed above, a larger magnetic moment usually corresponds to a deeper minimum. However, we can see that this is not really the case with the HLE16 and HLE17 functionals for Ni and Ni₃Al.

2. Nonmagnetic solids

We now turn to NM solids, but consider only elemental transition metals. In Table V we present those cases for which DFT can predict a FM ground state instead of the experimental NM ground state. Note that Refs. 22 and 24 reported that SCAN leads to a FM ground state for V and Pd. As we can see, in many cases disagreement with experiment is obtained. The worst cases are Sc and Pd for which all methods except LDA lead to a non-zero magnetic moment. LDA gives $\mu_S = 0$ and $\mu_S < 0.1 \mu_B$ for Sc and Pd, respectively. For the other systems, the functionals which usually lead to the correct NM state

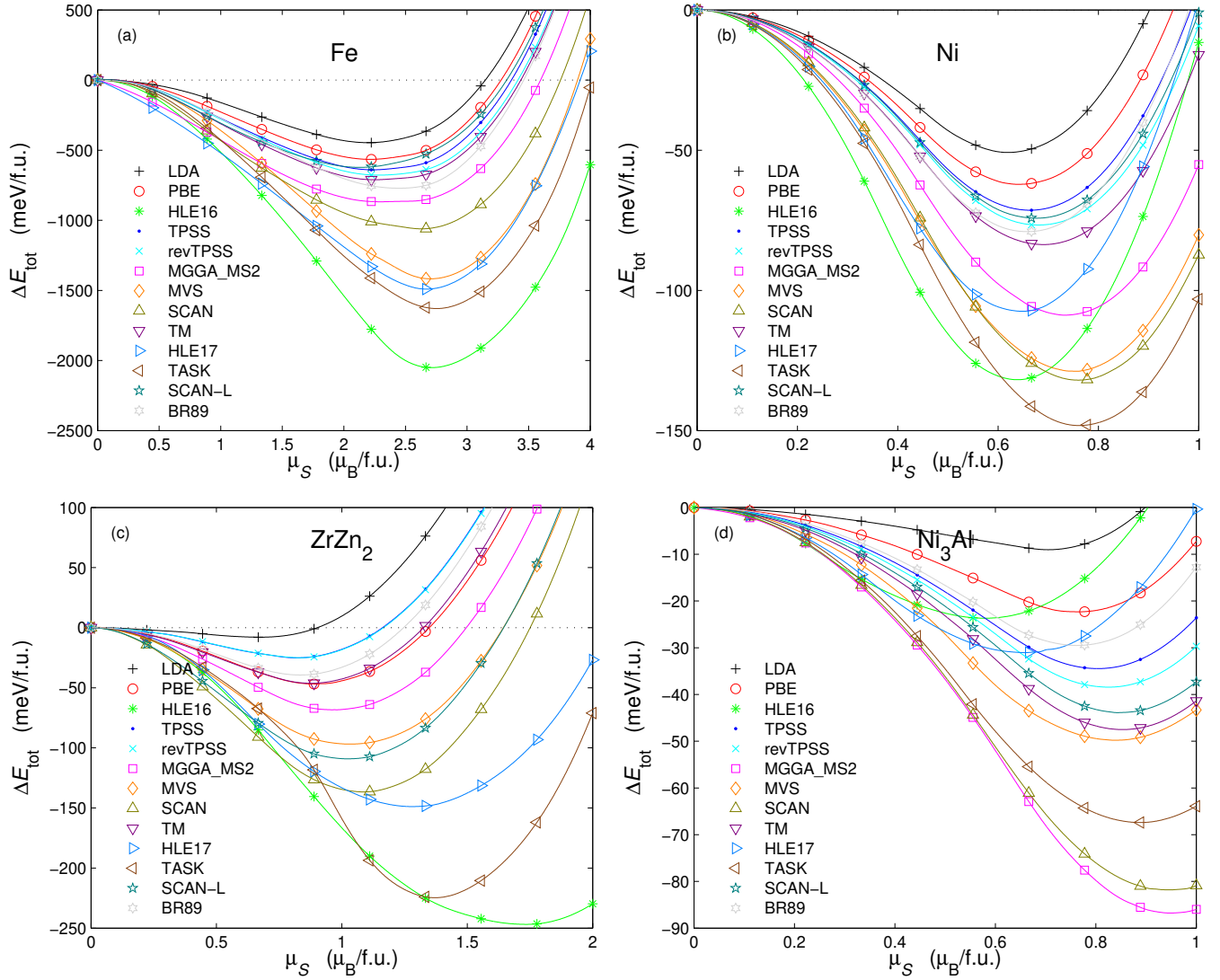


FIG. 1. Magnetic energy ΔE_{tot} as a function of the magnetic moment μ_S in Fe (a), Ni (b), ZrZn₂ (c), and Ni₃Al (d).

are LDA, PBE, TPSS, revTPSS, TM, and BR89. They were giving the least overestimations of the magnetic moment in FM systems. Note that the GGA HLE16 leads to extreme values, $2.86 \mu_B$, for Sc and Y, whereas the other functionals give values below $0.9 \mu_B$ for these two systems. Besides HLE16, TASK and HLE17 lead to the largest magnetic moments on average.

Figure 2 shows the magnetic energy for V as a function of μ_S . HLE16 leads to the deepest minimum, which was also the case for several of the FM solids, as seen above. SCAN leads to a very shallow minimum but a quite large moment of $0.55 \mu_B$, while SCAN-L and the other common MGGA's retain a NM state.

We mention that we also considered the possibility of an AFM ground state in Mo instead of the NM one. Mo belongs to the same group as Cr which is (incommensurate) AFM. By using a simple cubic two-atom CsCl cell, one functional, HLE16, leads to an AFM ground state

with an atomic moment of $0.54 \mu_B$ in the Bader volume. The other functionals lead to the correct NM phase.

3. Antiferromagnetic solids

The results for the spin atomic moment μ_S in AFM solids are shown in Table VI. We mention again that the Bader volume is used for the region defining the atomic moment. We also mention that for a comparison with experiment there is a possible non-negligible orbital contribution μ_L to the experimental value, and estimates are given in the caption of Table VI.

It is well known that LDA and PBE have the tendency to underestimate the moment in AFM oxides, as we observe here for most oxides. An exception is Cr₂O₃, since the LDA/PBE results lie in the range of the experimental values. In the cases of FeO and CoO, it is not possible to

TABLE V. Spin magnetic moment μ_S (in μ_B per formula unit) of (supposedly) NM solids. A non-zero μ_S means a FM ground state. The results for the MGGA functionals were obtained with the FSM method. The calculations were done at the geometry specified in Table I.

Method	Sc	V	Y	Pd	Pt
LDA	0.00	0.00	0.00	0.08	0.01
PBE	0.41	0.00	0.00	0.24	0.00
HLE16	2.86	0.78	2.86	0.36	0.51
mBJLDA	0.53	0.00	0.00	0.39	0.47
TPSS	0.39	0.00	0.00	0.29	0.01
revTPSS	0.37	0.01	0.01	0.30	0.00
MGGA_MS2	0.58	0.02	0.56	0.44	0.00
MVS	0.69	0.00	0.71	0.41	0.55
SCAN	0.62	0.55	0.60	0.44	0.08
TM	0.37	0.00	0.00	0.34	0.00
HLE17	0.86	0.61	0.76	0.38	0.42
TASK	0.80	0.64	0.79	0.43	0.37
SCAN-L	0.49	0.01	0.46	0.26	0.00
BR89	0.50	0.00	0.00	0.36	0.04

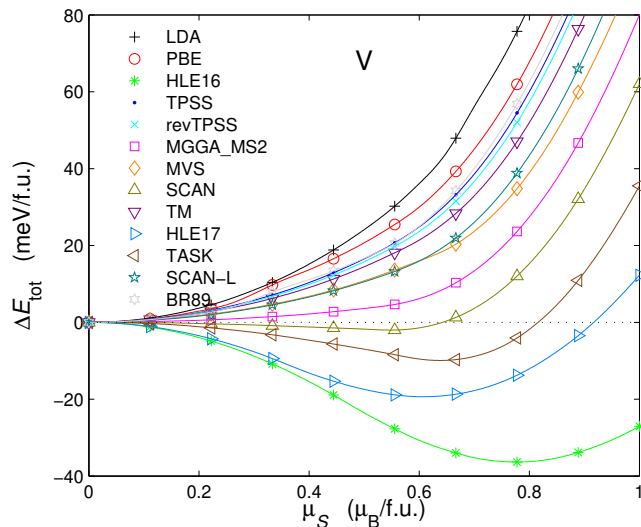


FIG. 2. Magnetic energy ΔE_{tot} as a function of the magnetic moment μ_S in V.

make a quantitative comparison with experiment since the range of experimental values and estimations for μ_L are large. For the intermetallic compounds CrSb and CrSb₂, where the magnetic moment on the Cr atom is considered (note that in CrSb₂ the moment on the Sb atom is non-zero, but tiny), PBE seems to lead to good agreement for CrSb, but to a very large overestimation of $\sim 0.8 \mu_B$ for CrSb₂. Such an overestimation by PBE for CrSb₂ has already been noted by Kuhn *et al.*,¹³⁶ who showed that by adding an on-site Hubbard correction to the Cr atom, using the around mean field (AMF) ver-

sion of PBE+ U ¹³⁷ with $U = 2.7$ eV and $J = 0.3$ eV, leads to a reduction of the moment from 2.57 to 2.03 μ_B (inside the Cr atomic sphere of radius 2.32 bohr). We could reproduce this trend with PBE+ U (AMF) (we get $\mu_S = 2.34 \mu_B$ inside the Bader volume). However, when using the fully localized limit (FLL)¹³⁷ variant of PBE+ U (with same U and J) the moment increases by $\sim 0.5 \mu_B$ with respect to PBE, and therefore worsens the agreement with experiment. These results with PBE+ U are not surprising since DFT+ U (AMF) is known to be better adapted than DFT+ U (FLL) for (near)-metallic systems which are not as correlated as TM oxides.^{138,139}

Compared to PBE, the GGA HLE16 significantly increases the magnetic moment for all systems except CuO, for which the PBE and HLE16 moments are curiously identical. The increase in μ_S is the largest for CrSb and CrSb₂ where it is clearly above 1 μ_B . Actually, among all methods HLE16 leads to (nearly) the largest value of μ_S for all systems except CoO, NiO, and CuO.

As observed in Sec. IIIB 1 for the FM solids, the MGGA TPSS, revTPSS, TM, SCAN-L, and BR89 lead to results that are relatively similar to PBE in most cases. These functionals lead to moments that are moderately larger than PBE, and the largest increase ($\sim 0.2 \mu_B$) occurs for Fe₂O₃, CrSb, and CrSb₂ with BR89. For the AFM solids considered here there is basically no case where a MGGA leads to a moment smaller than the PBE value, whereas there were many cases for the FM systems. All other MGGA lead to magnetic moments that are increased further, and the largest values of μ_S (disregarding the HLE16 results) are obtained in most cases by either TASK (MnO, FeO, CoO, and Fe₂O₃), HLE17 (Cr₂O₃, CrSb, and CrSb₂), or mBJLDA (NiO and CuO).

Due to the large uncertainties in the experimental values, a quantitative ranking of the theoretical methods is hardly possible. Overall, we can say that MGGA perform better than standard PBE. However, in some cases TPSS, revTPSS, TM, SCAN-L, and BR89 seem to be too weak, with magnetic moments that are still too small compared to experiment. On the other hand, HLE17 and TASK, as well as the GGA HLE16, lead to moments that are by far too large for Cr₂O₃ and the weakly correlated systems CrSb and CrSb₂. For the latter the overestimation of μ_S is in the range 1–2 μ_S with all functionals except PBE+ U (AMF). Finally, as already seen for the FM solids, HLE16 behaves erratically, since it leads to the smallest moment for CuO, but to the largest moment for some of the other AFM systems.

IV. DISCUSSION

A quite general observation that can be made from the results presented in Sec. IIIB is that if a MGGA functional increases (let us say with respect to PBE) magnetism in a system, then it will most likely do it in other magnetic systems, too. However, clear exceptions were noted with HLE16 and HLE17, which lead to rather er-

TABLE VI. Calculated spin atomic magnetic moment μ_S of the transition-metal atom (in μ_B and defined according to the Bader volume) of AFM solids compared to experimental values of the total atomic magnetic moment $\mu_S + \mu_L$. The orbital moment μ_L is estimated to be in the range 0.6-1 μ_B for FeO,¹⁰⁸⁻¹¹¹ 1-1.6 μ_B for CoO,¹⁰⁸⁻¹¹⁸ 0.3-0.45 μ_B for NiO,^{108,110,114,117,119} and much smaller in other oxides. No values of μ_L for CrSb and CrSb₂ could be found in the literature. The results for the MGGA functionals were obtained with the *C*-shift method [Eq. (1)]. The calculations were done at the geometry specified in Table I. The values which are in clear disagreement with experiment are underlined.

Method	MnO	FeO	CoO	NiO	CuO	Cr ₂ O ₃	Fe ₂ O ₃	CrSb	CrSb ₂
LDA	<u>4.33</u>	3.42	<u>2.38</u>	<u>1.20</u>	<u>0.12</u>	2.53	<u>3.42</u>	2.74	<u>2.64</u>
PBE	<u>4.39</u>	3.48	<u>2.45</u>	<u>1.37</u>	<u>0.37</u>	2.62	<u>3.61</u>	2.90	<u>2.75</u>
HLE16	<u>4.69</u>	3.67	2.59	1.45	<u>0.37</u>	<u>3.13</u>	4.08	<u>4.10</u>	<u>4.04</u>
mBJLDA	4.57	3.64	2.72	1.74	0.72	2.74	4.14	2.94	<u>2.73</u>
TPSS	<u>4.41</u>	3.52	2.50	1.46	0.45	2.63	3.74	2.97	<u>2.81</u>
revTPSS	<u>4.42</u>	3.53	2.51	1.46	0.45	2.64	3.78	3.00	<u>2.84</u>
MGGA_MS2	4.48	3.59	2.56	1.58	0.59	2.71	3.95	3.10	<u>2.95</u>
MVS	4.55	3.66	2.64	1.60	0.47	2.76	4.07	3.44	<u>3.28</u>
SCAN	4.53	3.62	2.60	1.60	0.57	2.73	4.01	3.32	<u>3.18</u>
TM	<u>4.42</u>	3.53	2.52	1.49	0.48	2.64	3.78	2.96	<u>2.79</u>
HLE17	4.62	3.65	2.63	1.56	0.49	<u>2.92</u>	4.05	<u>3.83</u>	3.74
TASK	4.63	3.70	2.67	1.60	0.50	<u>2.90</u>	4.18	<u>3.71</u>	<u>3.61</u>
SCAN-L	<u>4.43</u>	3.50	2.49	1.50	0.48	2.65	<u>3.71</u>	2.96	<u>2.79</u>
BR89	4.47	3.53	<u>2.44</u>	<u>1.42</u>	0.43	2.69	3.81	3.12	<u>2.98</u>
Expt.	4.58 ^a	3.32, ^b 4.2, ^c 4.6 ^d	3.35, ^e 3.8, ^{bf} 3.98 ^g	1.9, ^{ab} 2.2 ^{hi}	0.65 ^j	2.44, ^k 2.48, ^l 2.76 ^m	4.17, ⁿ 4.22 ^o	3.0 ^p	1.94 ^q

^a Ref. 120.

^b Ref. 121.

^c Ref. 122.

^d Ref. 123.

^e Ref. 124.

^f Ref. 125.

^g Ref. 126.

^h Ref. 119.

ⁱ Ref. 127.

^j Ref. 128.

^k Ref. 129.

^l Ref. 130.

^m Ref. 131.

ⁿ Ref. 132.

^o Ref. 133.

^p Ref. 134.

^q Ref. 135.

ratio results. The other general conclusion is that all tested MGGA lead in most cases to magnetic moments which are larger than the PBE values. In order to provide insight for some of the results, for instance by establishing a relation between the mathematical form of the xc functional and the magnetic moment μ_S , we consider the xc magnetic energy density

$$\Delta\epsilon_{xc}(\mathbf{r}) = \epsilon_{xc}^{(A)FM}(\mathbf{r}) - \epsilon_{xc}^{NM}(\mathbf{r}), \quad (3)$$

where $\epsilon_{xc}(\rho_\uparrow, \rho_\downarrow, \nabla\rho_\uparrow, \nabla\rho_\downarrow, \nabla^2\rho_\uparrow, \nabla^2\rho_\downarrow, t_\uparrow, t_\downarrow)$ is the xc-energy density defined as follows:

$$E_{xc} = \int \epsilon_{xc}(\mathbf{r}) d^3r. \quad (4)$$

In Eq. (3), $\epsilon_{xc}^{(A)FM}$ and ϵ_{xc}^{NM} were calculated in the (A)FM and NM phases, respectively. $\Delta\epsilon_{xc}$ is expected to be mainly negative in magnetic systems.

Figure 3 shows the difference in $\Delta\epsilon_{xc}$ between SCAN and SCAN-L ($\Delta\epsilon_{xc}^{SCAN-L} - \Delta\epsilon_{xc}^{SCAN}$) in the cases of the FM systems Fe and FeCo. Note that for a meaningful comparison, ϵ_{xc}^{FM} is calculated at the same value of μ_S for both functionals (2.0 and 4.5 μ_B for Fe and FeCo, respectively). As discussed in Sec. IIIB, SCAN-L reduces μ_S with respect to its parent SCAN. According to Fig. 3, this is mainly due to the large values of $\Delta\epsilon_{xc}^{SCAN-L} - \Delta\epsilon_{xc}^{SCAN}$ close to the atoms where $\Delta\epsilon_{xc}^{SCAN-L}$ is overall less negative than $\Delta\epsilon_{xc}^{SCAN}$ (this was checked by integrating only over the atomic region). The contribution to the integral of $\Delta\epsilon_{xc}^{SCAN-L} - \Delta\epsilon_{xc}^{SCAN}$ follows the 3d electron density, which in Fe has its maximum already at 0.5 bohr and quickly decays beyond 1.5 bohr, as shown in Fig. 4. The contribution from the interstitial region is one order of magnitude smaller and has opposite sign (negative), which is due to reverse polarization of the 4s electrons.^{84,85} Note

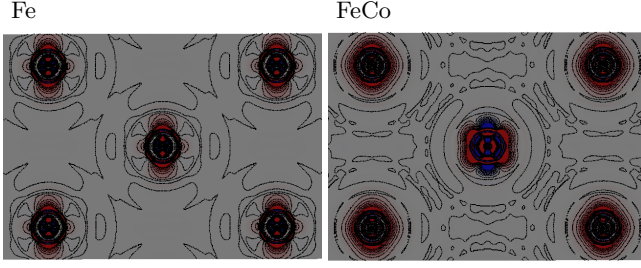


FIG. 3. Difference $\Delta\epsilon_{xc}^{\text{SCAN-L}} - \Delta\epsilon_{xc}^{\text{SCAN}}$ between the xc magnetic energy density obtained with SCAN and SCAN-L within a (110) plane in Fe (left panel) and FeCo (right panel, the middle atom is Co). The FM states correspond to $\mu_S = 2.0$ and $4.5 \mu_B$ for Fe and FeCo, respectively. Blue and red regions correspond to negative and positive values, respectively. The regions with the most intense blue/red colors correspond to absolute values above $0.02 \text{ Ry}/\text{bohr}^3$.

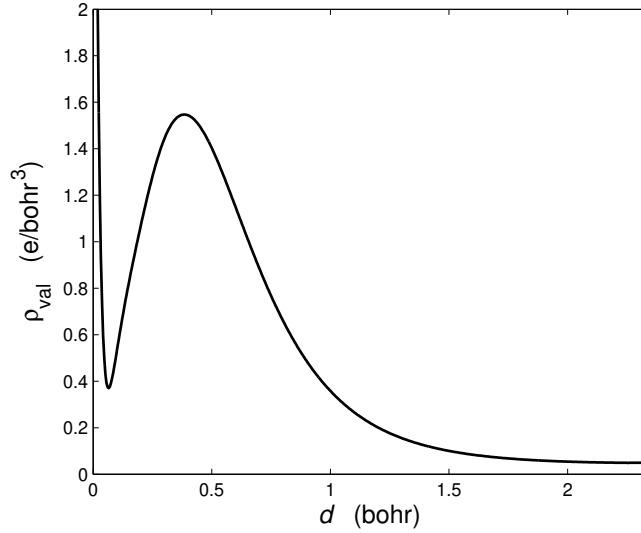


FIG. 4. Valence electron density $\rho_{\text{val}} = \rho_{\text{val}\uparrow} + \rho_{\text{val}\downarrow}$ in FM Fe plotted from the atom at (0,0,0) until the mid-distance to the atom at (1/2,1/2,1/2). The maximum near $d = 0.5 \text{ bohr}$ is due to the $3d$ electrons and the spike at the nucleus due to the $4s$ electrons.

that in general the difference $\Delta\epsilon_{xc}^{F1} - \Delta\epsilon_{xc}^{F2}$ around an atom between two functionals $F1$ and $F2$ is not uniformly positive or negative; there are lobes (which differentiate orbitals) with opposite signs. This is visible for the Co atom in FeCo, for instance. Of course, which lobes are the most visible also depends on the plane that is chosen for the plot. In Ref. 24 the case of Fe was explained by looking in detail at the differences between the iso-orbital indicator α_σ and its deorbitalized version $\alpha_{L,\sigma}$ (defined later) in the region around the nucleus corresponding to a sphere with a radius of 1.5 bohr , i.e., where $\Delta\epsilon_{xc}^{\text{SCAN-L}} - \Delta\epsilon_{xc}^{\text{SCAN}}$ is the largest. Later in the text we also provide a more detail discussion on the dif-

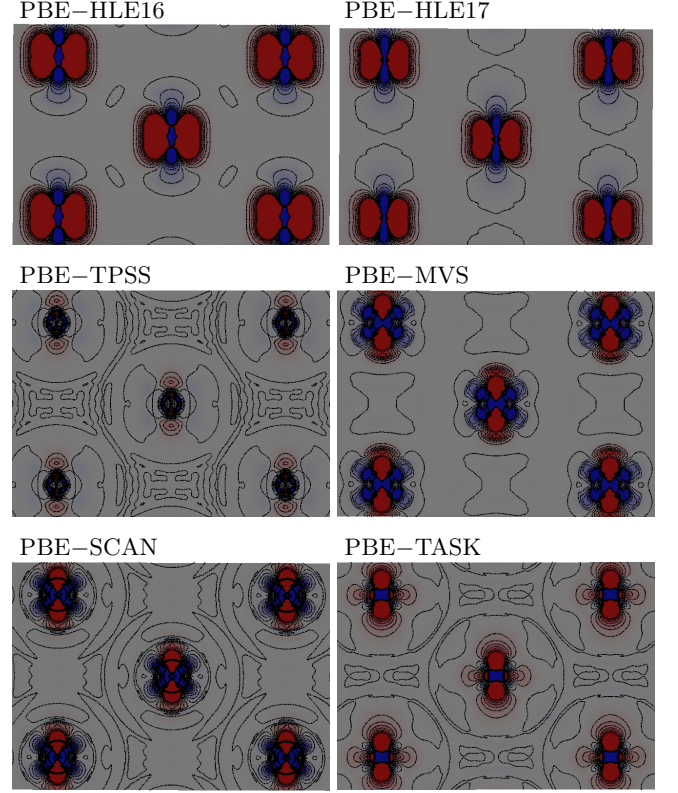


FIG. 5. Difference $\Delta\epsilon_{xc}^{\text{PBE}} - \Delta\epsilon_{xc}^F$ between the xc magnetic energy density within a (110) plane in Fe obtained with PBE and another functional F . The FM state corresponds to $\mu_S = 2.0 \mu_B$. Blue and red regions correspond to negative and positive values, respectively. The regions with the most intense blue/red colors correspond to absolute values above $0.02 \text{ Ry}/\text{bohr}^3$.

ference between α_σ and $\alpha_{L,\sigma}$ in Fe.

The MGGAs MVS, SCAN, HLE17, and TASK, and the GGA HLE16 lead to magnetic moments and magnetic energies that are usually clearly larger than the PBE value. For these functionals Fig. 5 shows for Fe the corresponding xc magnetic energy density in comparison to the one obtained with PBE. We can see that the empirical HLE16 and HLE17 functionals behave in a similar way and lead to a xc magnetic energy density that is more negative than PBE in larger regions of space (the red regions) and with different orientations of the lobes compared to the other functionals. However, it is important to mention that these differences between HLE16/HLE17 and the other functionals are actually mostly due to their corresponding xc potential (i.e., to self-consistency effects), which lead to different shape/occupation of the orbitals. This is demonstrated in Fig. 6 which compares $\Delta\epsilon_{xc}^{\text{PBE}} - \Delta\epsilon_{xc}^{\text{HLE17}}$ when $\Delta\epsilon_{xc}^{\text{HLE17}}$ is calculated with the density and KED obtained from either the mRPBE or the PBE potential. Very different patterns are obtained, and in the latter case $\Delta\epsilon_{xc}^{\text{PBE}} - \Delta\epsilon_{xc}^{\text{HLE17}}$ is very

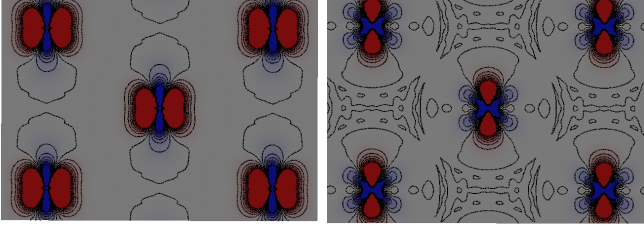


FIG. 6. Difference $\Delta\epsilon_{xc}^{\text{PBE}} - \Delta\epsilon_{xc}^{\text{HLE17}}$ between the xc magnetic energy density within a (110) plane in Fe obtained with PBE and HLE17. $\Delta\epsilon_{xc}^{\text{HLE17}}$ is evaluated with the density/KED generated from either the mRPBE (left panel) or the PBE potential (right panel). The FM state corresponds to $\mu_S = 2.0 \mu_B$. Blue and red regions correspond to negative and positive values, respectively. The regions with the most intense blue/red colors correspond to absolute values above 0.02 Ry/bohr^3 .

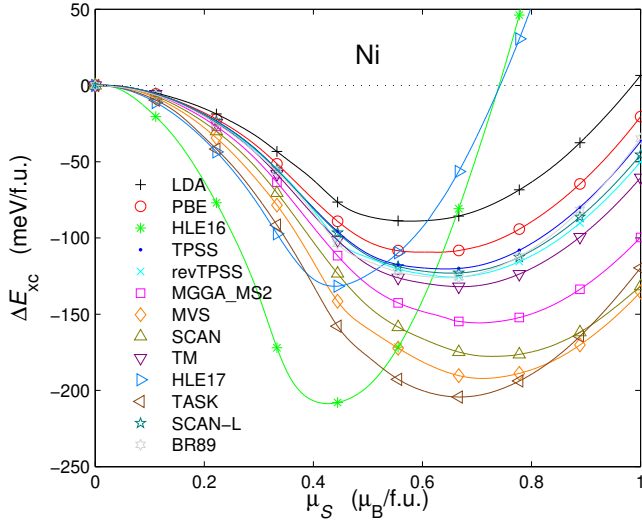


FIG. 7. xc magnetic energy ΔE_{xc} as a function of the magnetic moment μ_S in Ni.

similar to $\Delta\epsilon_{xc}^{\text{PBE}} - \Delta\epsilon_{xc}^{\text{MVS}}$ or $\Delta\epsilon_{xc}^{\text{PBE}} - \Delta\epsilon_{xc}^{\text{SCAN}}$, for instance. Nevertheless, despite the seemingly large influence of the density/KED on $\Delta\epsilon_{xc}^{\text{HLE17}}$, the results for μ_S and ΔE_{tot} change little. Indeed, using the density/KED generated from the PBE potential leads to $\mu_S = 2.71 \mu_B$ and $\Delta E_{\text{tot}} = -1441 \text{ meV/f.u.}$, which is quite similar to the results from Tables III and IV obtained with the mRPBE density/KED ($\mu_S = 2.67 \mu_B$ and $\Delta E_{\text{tot}} = -1491 \text{ meV/f.u.}$).

Besides HLE16/HLE17, TASK and TPSS (or TM which is similar) lead to negative regions that dominate the most and the least, respectively. This corroborates with the magnetic moment that is among the largest (smallest) with TASK (TPSS/TM).

Taking Ni as an example, Fig. 7 shows ΔE_{xc} as a function of μ_S . The shape and order of magnitude of the

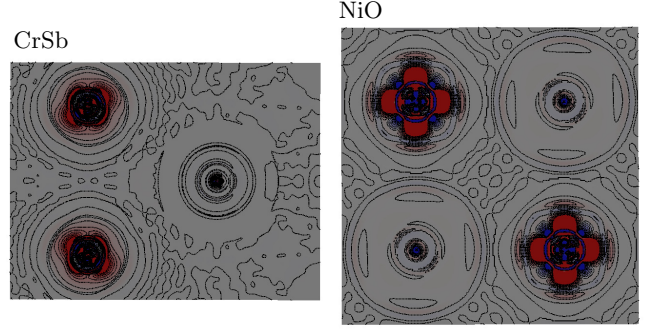


FIG. 8. Difference $\Delta\epsilon_{xc}^{\text{SCAN-L}} - \Delta\epsilon_{xc}^{\text{SCAN}}$ between the xc magnetic energy density obtained with SCAN and SCAN-L within a (110) plane in CrSb (left panel, the left atoms are Cr) and within a (100) plane in NiO (right panel, the upper left atom is Ni). The AFM states correspond to an atomic moment (defined according to the Bader volume) of $3.0 \mu_B$ (Cr) and $1.5 \mu_B$ (Ni). Blue and red regions correspond to negative and positive values, respectively. The regions with the most intense blue/red colors correspond to absolute values above 0.01 Ry/bohr^3 .

curves look rather similar to those of the total magnetic energy ΔE_{tot} [see Fig. 1(b)], which indicates that the other terms (kinetic energy and Coulomb) play a less important role. However, note that the magnitude of ΔE_{xc} is about 50 meV/f.u. larger than ΔE_{tot} . As already seen with ΔE_{tot} , the HLE16 and HLE17 functionals behave very differently from the other functionals. They lead to a minimum of the ΔE_{xc} curve which is at a much smaller value of the magnetic moment, however this effect is much less pronounced for the total magnetic energy ΔE_{tot} [Fig. 1(b)].

Figures 8 and 9 show $\Delta\epsilon_{xc}$ in the AFM systems CrSb and NiO. As for the FM systems, the difference $\Delta\epsilon_{xc}^{\text{SCAN-L}} - \Delta\epsilon_{xc}^{\text{SCAN}}$ in CrSb and NiO evidences the fact that SCAN leads to larger atomic moments than SCAN-L, since $\Delta\epsilon_{xc}^{\text{SCAN}}$ is overall more negative than $\Delta\epsilon_{xc}^{\text{SCAN-L}}$ on the transition-metal atoms. For CrSb on Fig. 9, we can see that $\Delta\epsilon_{xc}^{\text{PBE}} - \Delta\epsilon_{xc}^F$ is mostly positive on the Cr atom. In the case of HLE17, the regions corresponding to positive and negative values are in this plane (visually) roughly equal; nevertheless, around the Cr atoms the positive values of $\Delta\epsilon_{xc}^{\text{SCAN-L}} - \Delta\epsilon_{xc}^{\text{SCAN}}$ clearly dominate and represent about 70% of the integrated value (which is positive) of $\Delta\epsilon_{xc}^{\text{SCAN-L}} - \Delta\epsilon_{xc}^{\text{SCAN}}$ in the unit cell. In the case of TASK, the positive region largely dominates in this plane. We note again that HLE16, HLE17, and TASK lead to atomic moments of 4.10 , 3.83 , and $3.71 \mu_B$, respectively, which are much larger than $2.90 \mu_B$ from PBE. As discussed above for FM Fe, the magnitude of $\Delta\epsilon_{xc}^{\text{PBE}} - \Delta\epsilon_{xc}^F$ is the smallest for TPSS, which leads to a magnetic moment, $2.97 \mu_B$, very close to PBE.

It may also be interesting to compare the mathematical form of the xc-enhancement factor F_{xc} of the various

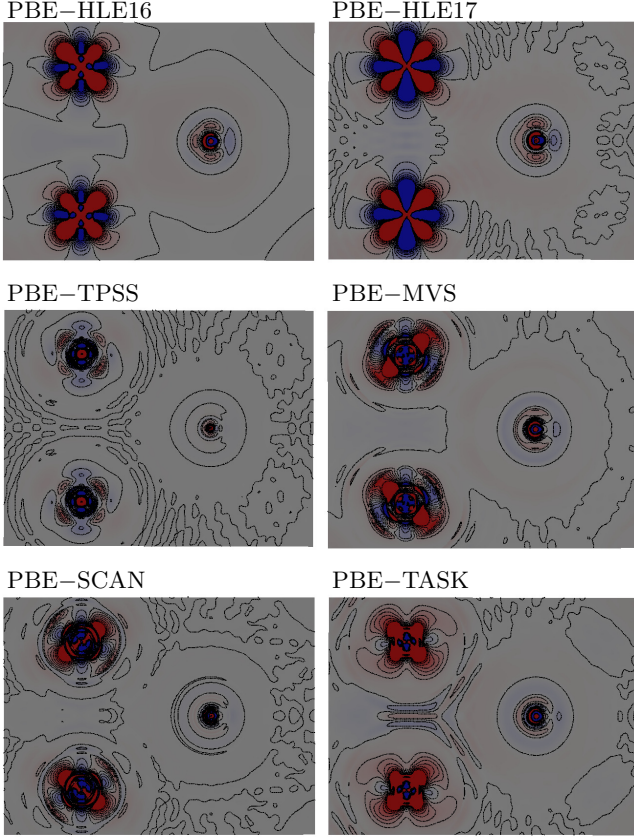


FIG. 9. Difference $\Delta\epsilon_{xc}^{PBE} - \Delta\epsilon_{xc}^F$ between the xc magnetic energy density within a (110) plane in CrSb obtained with PBE and another functional F . The AFM state corresponds to a Cr (left atoms) atomic moment of $\mu_S = 3.0 \mu_B$ (defined according to the Bader volume). Blue and red regions correspond to negative and positive values, respectively. The regions with the most intense blue/red colors correspond to absolute values above 0.01 Ry/bohr^3 .

functionals, which is defined as

$$F_{xc}(\mathbf{r}) = \frac{\epsilon_{xc}(\mathbf{r})}{\epsilon_x^{LDA}(\mathbf{r})}, \quad (5)$$

where (in spin-unpolarized formulation) $\epsilon_x^{LDA} = -(3/4)(3/\pi)^{1/3}\rho^{4/3}$ is the exchange energy density from LDA.¹ F_{xc} is usually expressed as a function of the Wigner-Seitz radius $r_s = (3/(4\pi\rho))^{1/3}$, reduced density gradient $s = |\nabla\rho| / (2(3\pi^2)^{1/3}\rho^{4/3})$, and iso-orbital indicator $\alpha = (t - t^W)/t^{TF}$, where $t^{TF} = (3/10)(3\pi^2)^{2/3}\rho^{5/3}$ and $t^W = |\nabla\rho|^2/(8\rho)$ are the Thomas-Fermi^{140,141} and von Weizsäcker¹⁴² KED, respectively.

In order to give an idea of the typical values of r_s , s , and α encountered in dense solids, and to make a relationship with the enhancement factors, Fig. 10 shows

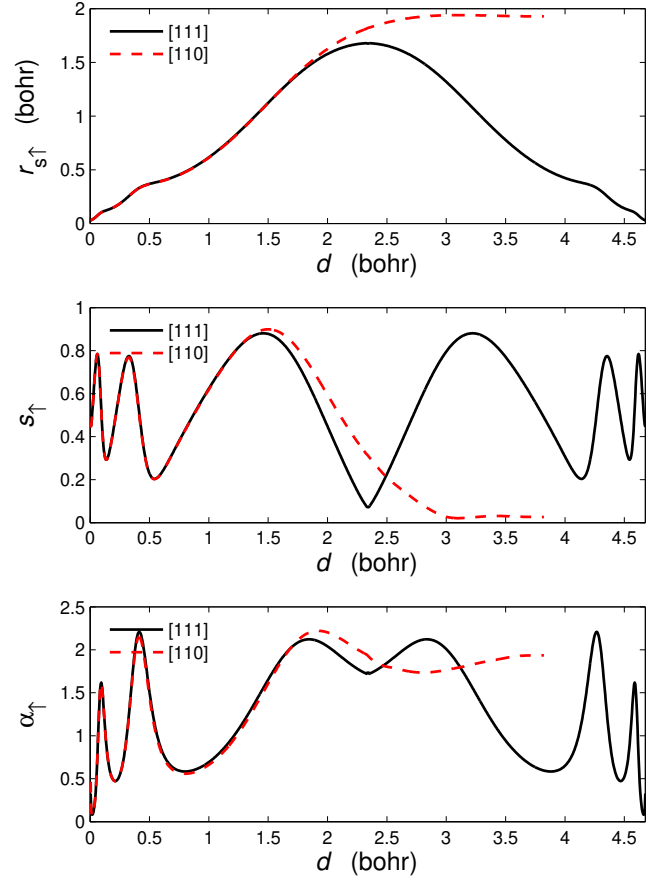


FIG. 10. $r_{s\sigma}$, s_σ , and α_σ for $\sigma = \uparrow$ (majority spin) as a function of the distance d for FM Fe plotted along the direction from (0,0,0) to (1/2,1/2,1/2) or (1/2,1/2,0).

plots of these quantities in FM Fe. Here, r_s ranges from 0 to 2, s from 0 to 1, and α from 0.5 to 2.5.

Figure 11 shows F_{xc} plotted as a function of s , α , or r_s for all functionals except SCAN-L and BR89. These two functionals depend on $\nabla^2\rho$, which does not allow a direct comparison with the other functionals. We can see that the enhancement factors of the GGA HLE16 and MGGA HLE17 have rather extreme shapes; both the value of F_{xc} and its derivative $\partial F_{xc}/\partial s$ are the largest. Such particular shapes of F_{xc} lead to xc potentials with very large oscillations⁵⁷ and therefore erratic and somehow unpredictable behavior. We also note that among the MGGA, TPSS, revTPSS, and TM have the weakest dependency on α and behave nearly like GGAs. In contrast to them, F_{xc} from the TASK functional has by far the strongest variation with respect to α , so that starting at some value of α it becomes the smallest enhancement factor among all those considered in this work. As discussed below, this particular behavior of the enhancement factor of TASK, as well as the ones from SCAN and MVS which show a similar feature, is related to the large magnetic moments obtained with these functionals. Actually, for these three functionals, as well as HLE16 for small values of s , Fig. 11

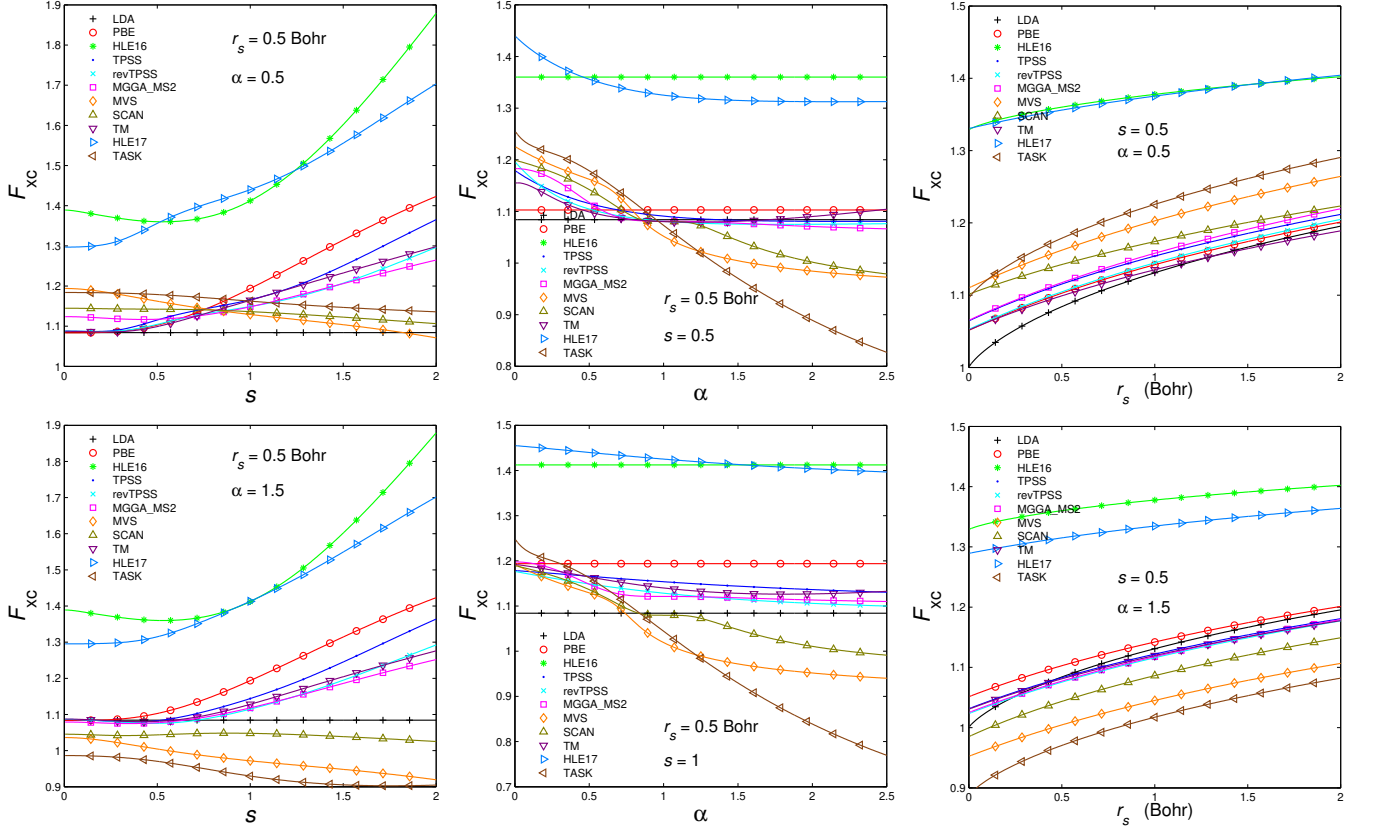


FIG. 11. Enhancement factors F_{xc} plotted as a function of s (left panels), α (middle panels), or r_s (right panels). The value of the two other variables (that are kept fixed) are indicated in the respective panels. Note the different scales on the vertical axis.

shows that $\partial F_{xc}/\partial s$ is also negative. The r_s -dependency of the LDA and TASK enhancement factors are also particular; depending on the value of s and/or α , they increase faster than for all other functionals.

As a side note, we mention that a few additional calculations were done by combining exchange of one functional (e.g., SCAN) with correlation of another functional (e.g., TPSS). From the results (not shown), we concluded that the choice of correlation has a rather minor effect on the magnetic moment.

MGGAs can be very different to each other in terms of enhancement factor and xc magnetic energy density. Thus, the details of the mechanism leading to an increase of the magnetic moment (with respect to PBE) may also differ from one functional to the other. For instance, the two MGGAs HLE17 and TASK lead (albeit not always with HLE17) to large magnetic moments, despite they have extremely different analytical forms. As discussed above and in Ref. 24, the analytical form of a functional for densities close to the transition-metal atom determines the magnetic moment. This is of course expected since this is where the $3d$ electrons are located, as shown in Fig. 4 for FM Fe. Figure 12 shows the averages of $r_{s,\sigma}$, s_σ , α_σ , and $\alpha_{L,\sigma}$ in a sphere of radius 1.25 bohr surrounding an atom in FM Fe plotted as function of the

magnetic moment μ_S . We can see that for the majority spin ($\sigma = \uparrow$) $\langle r_{s,\uparrow} \rangle$, $\langle s_\uparrow \rangle$, $\langle \alpha_\uparrow \rangle$ decrease when μ_S increases. We just note that starting at $\mu_S \sim 3 \mu_B$ $\langle \alpha_\uparrow \rangle$ increases, which is however not relevant since $3 \mu_B$ is larger than what all functionals give for Fe. For the minority spin $\sigma = \downarrow$, the trends are more or less the opposite.

Relating Fig. 12 with the results for the magnetic moment, $\langle \alpha_\sigma \rangle$ is particularly relevant for TASK, SCAN, and MVS as explained in the following. When μ_S increases, $\langle \alpha_\uparrow \rangle$ and $\langle \alpha_\downarrow \rangle$ decrease and increase, respectively. Since the derivatives $\partial F_{xc}/\partial \alpha$ of these three MGGAs are negative (see Fig. 11), an increase of μ_S leads to an increase and decrease of the $\sigma = \uparrow$ and $\sigma = \downarrow$ exchange enhancement factors, respectively. Thus, a negative $\partial F_{xc}/\partial \alpha$ contributes to an increase of the exchange splitting. This is not the case with TPSS, revTPSS, or TM which have a very weak dependency on α . This is a very plausible explanation since TASK, SCAN, and MVS lead to some of the largest moments, while TPSS, revTPSS, and TM to the smallest. The same mechanism, but probably weaker, can be invoked with $\langle s_\sigma \rangle$ since $\partial F_{xc}/\partial s$ is negative also only for TASK, SCAN, and MVS.

Aschebrock and Kümmel⁴⁹ showed that having a negative slope $\partial F_x/\partial \alpha$ leads to two desirable features: (a) the presence of a field-counteracting term in the potential

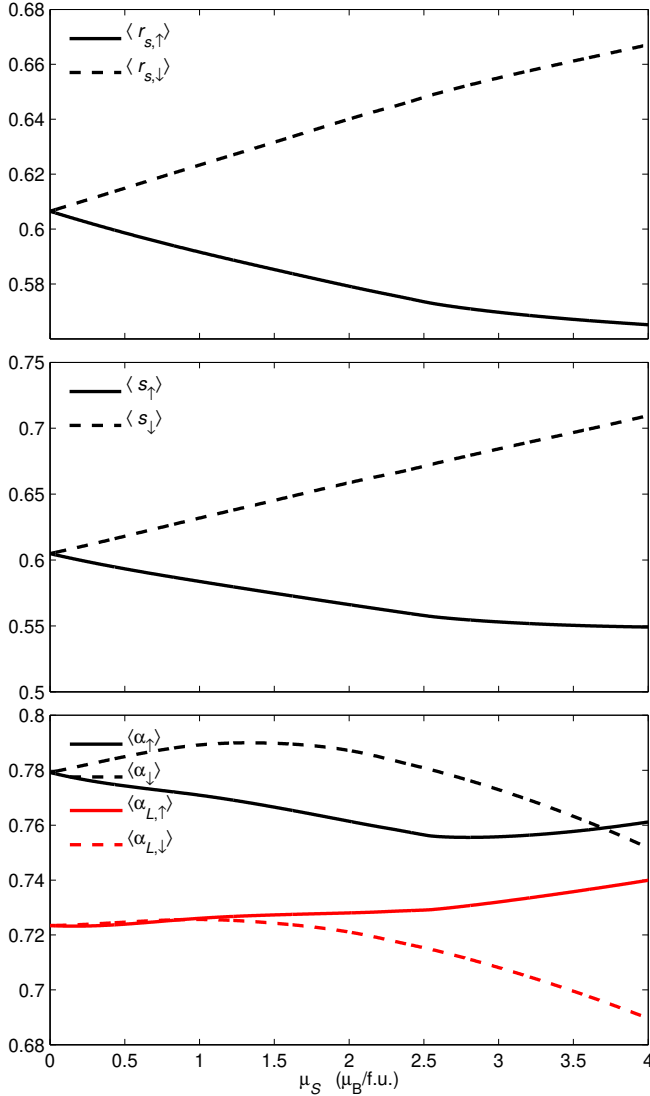


FIG. 12. Spatial average of $r_{s,\sigma}$, s_σ , α_σ , and $\alpha_{L,\sigma}$ inside a sphere of radius 1.25 bohr centered on the atom in Fe plotted as a function of μ_S . $\sigma = \uparrow$ corresponds to the majority spin.

(as with exact exchange) and (b) a derivative discontinuity that is larger and therefore leads to more accurate band gaps. However, in the present context, magnetism, a negative value of $\partial F_x/\partial\alpha$ does not seem to be beneficial. Thus, MGGAs with such negative $\partial F_x/\partial\alpha$ to a certain extent mimic exact exchange, which also leads to too large magnetic moments in FM metals.^{143,144} It was argued that a negative slope $\partial F_x/\partial\alpha$ increases the nonlocal character of the MGA exchange.⁴⁹ A possible way to cure the over-magnetization problem of TASK or SCAN would be to combine the exchange component with a more compatible (and most likely more advanced) correlation component. In the case of exact exchange, *ab initio* correlations can solve some of the problems of exact exchange.

Mejía-Rodríguez and Trickey²⁴ provided an explana-

tion for the smaller moment obtained with SCAN-L compared to SCAN. Here, a similar explanation is provided but with an emphasis on the importance of $\partial F_{xc}/\partial\alpha$ as discussed above. Compared to α_σ , the deorbitalized $\alpha_{L,\sigma}$ is smaller in magnitude for both spins, as shown in Fig. 12. Another important difference can be noted; for the majority spin $\sigma = \uparrow$, $\langle\alpha_{L,\uparrow}\rangle$ increases with μ_S instead of decreasing, while for the minority spin, the increase for small values of μ_S is strongly reduced. Therefore, by substituting α_σ by $\alpha_{L,\sigma}$ in TASK, SCAN, or MVS, the effect on the exchange splitting due to $\partial F_{xc}/\partial\alpha$ is strongly suppressed (or maybe even reversed), which explains the reduction of magnetism. Actually, a deorbitalization of TPSS leads to very small change in the results (see Ref. 24), which is due to the very weak dependency of TPSS on α .

SCAN-L has been shown to be more appropriate than SCAN for magnetic and non-magnetic itinerant metals.²⁴ However, the $\nabla^2\rho$ -dependency of SCAN-L may also carry practical disadvantages, since implementations of this family of functionals are less common than for *t*-MGGAs. Furthermore, the third and fourth derivatives of the density, that are required for the potential, may lead to numerical problems.^{32,145–147} Therefore, it would be interesting to find a *t*-dependent alternative to SCAN-L, that is, a slightly modified SCAN that leads to minimal changes for the geometries and binding energies, but reduces the magnetic moment. Mejía-Rodríguez and Trickey²⁴ reported such attempts, which were apparently unsuccessful. Our numerous own attempts have all remained unsuccessful, as well. The most simple ones consist of just changing the value of one of the parameters in SCAN. Among them, c_{1x} for instance, can be used to vary the switching function and thus the magnetic moment (see Ref. 24). By increasing the value of c_{1x} above ~ 2.5 ($c_{1x} = 0.667$ in SCAN), the magnetic moments of Fe, Co, and Ni get smaller and approach to some extent the SCAN-L values. As discussed above, a negative slope $\partial F_{xc}/\partial\alpha$ favors a large moment. Since an increase of c_{1x} makes $\partial F_{xc}/\partial\alpha$ less negative for values of α below 1, this should be (one of) the main reason(s) why the moments are smaller. However, with such values for c_{1x} , the errors for the lattice constant and cohesive energy (results now shown) are larger (by $\sim 50\%$) than SCAN. Another strategy that we have considered consists of slightly modifying the expression of α in SCAN. Numerous expressions have been tried, but none of them was useful to achieve our goal. A modification of α can work for a system, but not for another. Thus, the construction of a *t*-MGA with similar performance as SCAN-L seems far from trivial, as already reported by Mejía-Rodríguez and Trickey.²⁴

V. SUMMARY

The focus of this work has been on the description of magnetism in solids with MGA functionals. FM, NM, and AFM systems have been considered. The goal was

to provide an overview of the reliability of MGGA and the possible improvement with respect to standard GGA functionals like PBE. The most important observations are the following. In the vast majority of cases, the tested MGGA functionals lead to a magnetic moment that is larger than the value obtained with LDA and PBE. This means that for the considered FM systems, which are itinerant metals, the agreement with experiment can only be worse than with LDA and PBE, which are known to already slightly (or even strongly when spin fluctuations are important) overestimate the magnetic moment in FM solids. Consistent with this trend, a certain number of NM metals can be wrongly described as FM with MGGA, and already with PBE in some cases. In the case of the AFM oxides with localized $3d$ electrons, using a MGGA leads to a more realistic value of the atomic moment, since PBE leads to too small moments. Only in the case of Cr_2O_3 the LDA and PBE values seem to be within the experimental range. Concerning the weakly correlated AFM CrSb and CrSb_2 , PBE is in agreement with experiment for the former, but strongly overestimates the moment for the latter. Therefore, using a MGGA does not really seem to be beneficial for such systems.

The MGGA that we have considered can be split into two groups. Those which give results that are qualitatively similar to PBE, namely BR89, TPSS, revTPSS, TM, and SCAN-L. They lead to reasonable results for metals, but clearly underestimate the atomic magnetic moment in the AFM transition-metal oxides. The other group consists of TASK, HLE17, SCAN, MVS, and MGGA_MS2, which lead to sizeably larger moments. For the FM metals, TASK, SCAN, and MVS lead in many cases to the largest magnetic moments, and therefore the largest disagreement with experiment. They also lead to a non-zero magnetic moment for the NM metals that we have considered. For the AFM systems, TASK, HLE17, as well as the mBJLDA potential and the GGA HLE16 lead to the largest values of the atomic moment. As just mentioned above, this is beneficial for the transition-

metal oxides, but not for the weakly correlated CrSb and CrSb_2 . We have also shown that HLE16 and HLE17 lead to erratic and unpredictable results. As a final short conclusion, no GGA and no MGGA leads to satisfying results, even qualitatively, for itinerant metals and strongly correlated AFM oxides at the same time. One goal that we have not been able to achieve is to propose a *non-deorbitalized* modification of SCAN that is good for the magnetic moment of metals, while keeping the accuracy of SCAN for other properties like the lattice constant.

In an attempt to provide an analysis of some of the observed trends, the xc magnetic energy density was visualized and the analytical form of the functionals compared. Some of the functionals, HLE16, HLE17, and TASK, have very unusual shape for their enhancement factor. However, it is not necessary to use a functional with such an enhancement factor to get increased magnetism compared to PBE; other functionals like SCAN or MVS also lead to larger magnetic moments. Actually, we deduced that a negative derivative $\partial F_{xc}/\partial\alpha$ of the enhancement factor should contribute in making the magnetic moment larger, since the iso-orbital indicator α of the majority (minority) spin decreases (increases) with the moment, leading to an enhanced exchange splitting.

On a more technical side, we have also discussed the choice of the GGA potential for generating the orbitals plugged into the MGGA functionals. We have shown that when an appropriate GGA potential is chosen, the results are very close to those obtained (from another code) self-consistently. We also pointed out the importance of choosing an atomic volume for the magnetic moment in AFM systems that is large enough, for which we used the basin as defined in Bader's QTAIM.

ACKNOWLEDGMENTS

P.B. acknowledges support from the Austrian Science Foundation (FWF) for Project W1243 (Solids4Fun).

-
- ¹ W. Kohn and L. J. Sham, Phys. Rev. **140**, A1133 (1965).
 - ² A. D. Becke, Phys. Rev. A **38**, 3098 (1988).
 - ³ J. P. Perdew, J. A. Chevary, S. H. Vosko, K. A. Jackson, M. R. Pederson, D. J. Singh, and C. Fiolhais, Phys. Rev. B **46**, 6671 (1992), **48**, 4978(E) (1993).
 - ⁴ P. Hohenberg and W. Kohn, Phys. Rev. **136**, B864 (1964).
 - ⁵ B. Barbiellini, E. G. Moroni, and T. Jarlborg, J. Phys.: Condens. Matter **2**, 7597 (1990).
 - ⁶ D. J. Singh, W. E. Pickett, and H. Krakauer, Phys. Rev. B **43**, 11628 (1991).
 - ⁷ S. Sharma, E. K. U. Gross, A. Sanna, and J. K. Dewhurst, J. Chem. Theory Comput. **14**, 1247 (2018).
 - ⁸ J. P. Perdew and A. Zunger, Phys. Rev. B **23**, 5048 (1981).
 - ⁹ K. Terakura, T. Oguchi, A. R. Williams, and J. Kübler, Phys. Rev. B **30**, 4734 (1984).
 - ¹⁰ T. Van Voorhis and G. E. Scuseria, J. Chem. Phys. **109**, 400 (1998), **129**, 219901 (2008).
 - ¹¹ V. N. Staroverov, G. E. Scuseria, J. Tao, and J. P. Perdew, J. Chem. Phys. **119**, 12129 (2003), **121**, 11507 (2004).
 - ¹² V. N. Staroverov, G. E. Scuseria, J. Tao, and J. P. Perdew, Phys. Rev. B **69**, 075102 (2004), **78**, 239907(E) (2008).
 - ¹³ J. Sun, A. Ruzsinszky, and J. P. Perdew, Phys. Rev. Lett. **115**, 036402 (2015).
 - ¹⁴ F. Tran, J. Stelzl, and P. Blaha, J. Chem. Phys. **144**, 204120 (2016).
 - ¹⁵ Y. Zhang, D. A. Kitchaev, J. Yang, T. Chen, S. T. Dacek, R. A. Sarmiento-Pérez, M. A. L. Marques, H. Peng, G. Ceder, J. P. Perdew, and J. Sun, npj Comput. Mater. **4**, 9 (2018).
 - ¹⁶ E. B. Isaacs and C. Wolverton, Phys. Rev. Materials **2**, 063801 (2018).
 - ¹⁷ H. Peng, Z.-H. Yang, J. P. Perdew, and J. Sun, Phys.

- Rev. X **6**, 041005 (2016).
- ¹⁸ J. G. Brandenburg, J. E. Bates, J. Sun, and J. P. Perdew, Phys. Rev. B **94**, 115144 (2016).
 - ¹⁹ F. Tran, L. Kalantari, B. Traoré, X. Rocquefelte, and P. Blaha, Phys. Rev. Materials **3**, 063602 (2019).
 - ²⁰ S. Jana, A. Patra, and P. Samal, J. Chem. Phys. **149**, 044120 (2018).
 - ²¹ M. Ekholm, D. Gambino, H. J. M. Jönsson, F. Tasnádi, B. Alling, and I. A. Abrikosov, Phys. Rev. B **98**, 094413 (2018).
 - ²² Y. Fu and D. J. Singh, Phys. Rev. Lett. **121**, 207201 (2018).
 - ²³ Y. Fu and D. J. Singh, Phys. Rev. B **100**, 045126 (2019).
 - ²⁴ D. Mejía-Rodríguez and S. B. Trickey, Phys. Rev. B **100**, 041113(R) (2019).
 - ²⁵ A. H. Romero and M. J. Verstraete, Eur. Phys. J. B **91**, 193 (2018).
 - ²⁶ V. D. Buchelnikov, V. V. Sokolovskiy, O. N. Miroshkina, M. A. Zagrebin, J. Nokelainen, A. Pulkkinen, B. Barbiellini, and E. Lähderanta, Phys. Rev. B **99**, 014426 (2019).
 - ²⁷ S. Shepard and M. Smeu, J. Chem. Phys. **150**, 154702 (2019).
 - ²⁸ J. Tao, J. P. Perdew, V. N. Staroverov, and G. E. Scuseria, Phys. Rev. Lett. **91**, 146401 (2003).
 - ²⁹ J. P. Perdew, A. Ruzsinszky, G. I. Csonka, L. A. Constantin, and J. Sun, Phys. Rev. Lett. **103**, 026403 (2009), **106**, 179902 (2011).
 - ³⁰ J. Tao and Y. Mo, Phys. Rev. Lett. **117**, 073001 (2016).
 - ³¹ J. Sun, M. Marsman, G. I. Csonka, A. Ruzsinszky, P. Hao, Y.-S. Kim, G. Kresse, and J. P. Perdew, Phys. Rev. B **84**, 035117 (2011).
 - ³² D. Mejia-Rodriguez and S. B. Trickey, Phys. Rev. A **96**, 052512 (2017).
 - ³³ D. Mejia-Rodriguez and S. B. Trickey, Phys. Rev. B **98**, 115161 (2018).
 - ³⁴ F. Tran, P. Kovács, L. Kalantari, G. K. H. Madsen, and P. Blaha, J. Chem. Phys. **149**, 144105 (2018).
 - ³⁵ G. Sai Gautam and E. A. Carter, Phys. Rev. Materials **2**, 095401 (2018).
 - ³⁶ O. Y. Long, G. Sai Gautam, and E. A. Carter, Phys. Rev. Materials **4**, 045401 (2020).
 - ³⁷ B. Xiao, J. Sun, A. Ruzsinszky, and J. P. Perdew, Phys. Rev. B **90**, 085134 (2014).
 - ³⁸ I. Kylänpää, J. Balachandran, P. Ganesh, O. Heinonen, P. R. C. Kent, and J. T. Krogel, Phys. Rev. Materials **1**, 065408 (2017).
 - ³⁹ J. Sun, B. Xiao, and A. Ruzsinszky, J. Chem. Phys. **137**, 051101 (2012).
 - ⁴⁰ J. Sun, R. Haunschuld, B. Xiao, I. W. Bulik, G. E. Scuseria, and J. P. Perdew, J. Chem. Phys. **138**, 044113 (2013).
 - ⁴¹ C. Lane, J. W. Furness, I. G. Buda, Y. Zhang, R. S. Markiewicz, B. Barbiellini, J. Sun, and A. Bansil, Phys. Rev. B **98**, 125140 (2018).
 - ⁴² Y. Zhang, J. Furness, R. Zhang, Z. Wang, A. Zunger, and J. Sun, arXiv e-prints, arXiv:1906.06467 (2019).
 - ⁴³ A. Pulkkinen, B. Barbiellini, J. Nokelainen, V. Sokolovskiy, D. Baigutlin, O. Miroshkina, M. Zagrebin, V. Buchelnikov, C. Lane, R. S. Markiewicz, A. Bansil, J. Sun, K. Pussi, and E. Lähderanta, Phys. Rev. B **101**, 075115 (2020).
 - ⁴⁴ F. Tran, D. Koller, and P. Blaha, Phys. Rev. B **86**, 134406 (2012).
 - ⁴⁵ F. Della Sala, E. Fabiano, and L. A. Constantin, Int. J. Quantum Chem. **116**, 1641 (2016).
 - ⁴⁶ A. D. Becke and M. R. Roussel, Phys. Rev. A **39**, 3761 (1989).
 - ⁴⁷ J. Sun, J. P. Perdew, and A. Ruzsinszky, Proc. Natl. Acad. Sci. U.S.A. **112**, 685 (2015).
 - ⁴⁸ P. Verma and D. G. Truhlar, J. Phys. Chem. C **121**, 7144 (2017).
 - ⁴⁹ T. Aschebrock and S. Kümmel, Phys. Rev. Research **1**, 033082 (2019).
 - ⁵⁰ J. P. Perdew and Y. Wang, Phys. Rev. B **45**, 13244 (1992), **98**, 079904(E) (2018).
 - ⁵¹ J. P. Perdew and L. A. Constantin, Phys. Rev. B **75**, 155109 (2007).
 - ⁵² A. V. Bienvenu and G. Knizia, J. Chem. Theory Comput. **14**, 1297 (2018).
 - ⁵³ F. Tran and P. Blaha, Phys. Rev. Lett. **102**, 226401 (2009).
 - ⁵⁴ J. P. Perdew, K. Burke, and M. Ernzerhof, Phys. Rev. Lett. **77**, 3865 (1996), **78**, 1396(E) (1997).
 - ⁵⁵ P. Verma and D. G. Truhlar, J. Phys. Chem. Lett. **8**, 380 (2017).
 - ⁵⁶ A. D. Boese and N. C. Handy, J. Chem. Phys. **114**, 5497 (2001).
 - ⁵⁷ F. Tran and P. Blaha, J. Phys. Chem. A **121**, 3318 (2017).
 - ⁵⁸ P. Borlido, T. Aull, A. W. Huran, F. Tran, M. A. L. Marques, and S. Botti, J. Chem. Theory Comput. **15**, 5069 (2019).
 - ⁵⁹ F. Tran, J. Doumont, L. Kalantari, A. W. Huran, M. A. L. Marques, and P. Blaha, J. Appl. Phys. **126**, 110902 (2019).
 - ⁶⁰ P. Blaha, K. Schwarz, G. K. H. Madsen, D. Kvasnicka, J. Luitz, R. Laskowski, F. Tran, and L. D. Marks, *WIEN2k: An Augmented Plane Wave plus Local Orbitals Program for Calculating Crystal Properties* (Vienna University of Technology, Austria, 2018).
 - ⁶¹ P. Blaha, K. Schwarz, F. Tran, R. Laskowski, G. K. H. Madsen, and L. D. Marks, J. Chem. Phys. **152**, 074101 (2020).
 - ⁶² O. K. Andersen, Phys. Rev. B **12**, 3060 (1975).
 - ⁶³ D. J. Singh and L. Nordström, *Planewaves, Pseudopotentials, and the LAPW Method, 2nd ed.* (Springer, New York, 2006).
 - ⁶⁴ F. Karsai, F. Tran, and P. Blaha, Comput. Phys. Commun. **220**, 230 (2017).
 - ⁶⁵ M. A. L. Marques, M. J. T. Oliveira, and T. Burnus, Comput. Phys. Commun. **183**, 2272 (2012).
 - ⁶⁶ S. Lehtola, C. Steigemann, M. J. T. Oliveira, and M. A. L. Marques, SoftwareX **7**, 1 (2018).
 - ⁶⁷ K. Schwarz and P. Mohn, J. Phys. F: Met. Phys. **14**, L129 (1984).
 - ⁶⁸ F. Tran, J. Doumont, P. Blaha, M. A. L. Marques, S. Botti, and A. P. Bartók, J. Chem. Phys. **151**, 161102 (2019).
 - ⁶⁹ B. Hammer, L. B. Hansen, and J. K. Nørskov, Phys. Rev. B **59**, 7413 (1999).
 - ⁷⁰ E. Engel and S. H. Vosko, Phys. Rev. B **47**, 13164 (1993).
 - ⁷¹ G. Kresse and J. Furthmüller, Phys. Rev. B **54**, 11169 (1996).
 - ⁷² J. Enkovaara, C. Rostgaard, J. J. Mortensen, J. Chen, M. Dulak, L. Ferrighi, J. Gavnholt, C. Glinsvad, V. Haikola, H. A. Hansen, H. H. Kristoffersen, M. Kuisma, A. H. Larsen, L. Lehtovaara, M. Ljungberg, O. Lopez-Acevedo, P. G. Moses, J. Ojanen, T. Olsen, V. Petzold, N. A. Romero, J. Stausholm-Møller, M. Strange, G. A.

- Tritsaridis, M. Vanin, M. Walter, B. Hammer, H. Häkkinen, G. K. H. Madsen, R. M. Nieminen, J. K. Nørskov, M. Puska, T. T. Rantala, J. Schiøtz, K. S. Thygesen, and K. W. Jacobsen, *J. Phys.: Condens. Matter* **22**, 253202 (2010).
- ⁷³ L. Ferrighi, G. K. H. Madsen, and B. Hammer, *J. Chem. Phys.* **135**, 084704 (2011).
- ⁷⁴ P. E. Blöchl, *Phys. Rev. B* **50**, 17953 (1994).
- ⁷⁵ R. F. W. Bader, *Atoms in Molecules: A Quantum Theory* (Oxford University Press, Oxford, 1990).
- ⁷⁶ R. F. W. Bader, *Chem. Rev.* **91**, 893 (1991).
- ⁷⁷ A. Otero-de-la-Roza, M. A. Blanco, A. Martín Pendás, and V. Luaña, *Comput. Phys. Commun.* **180**, 157 (2009).
- ⁷⁸ A. Otero-de-la-Roza, E. R. Johnson, and V. Luaña, *Comput. Phys. Commun.* **185**, 1007 (2014).
- ⁷⁹ G. Bergerhoff, R. Hundt, R. Sievers, and I. D. Brown, *J. Chem. Inf. Comput. Sci.* **23**, 66 (1983).
- ⁸⁰ A. Belsky, M. Hellenbrandt, V. L. Karen, and P. Luksch, *Acta Cryst.* **B58**, 364 (2002).
- ⁸¹ C. T. Chen, Y. U. Idzerda, H.-J. Lin, N. V. Smith, G. Meigs, E. Chaban, G. H. Ho, E. Pellegrin, and F. Sette, *Phys. Rev. Lett.* **75**, 152 (1995).
- ⁸² A. Scherz, Ph.D. thesis, Free University of Berlin (2003).
- ⁸³ R. A. Reck and D. L. Fry, *Phys. Rev.* **184**, 492 (1969).
- ⁸⁴ R. M. Moon, *Phys. Rev.* **136**, A195 (1964).
- ⁸⁵ H. A. Mook and C. G. Shull, *J. Appl. Phys.* **37**, 1034 (1966).
- ⁸⁶ E. Di Fabrizio, G. Mazzone, C. Petrillo, and F. Sacchetti, *Phys. Rev. B* **40**, 9502 (1989).
- ⁸⁷ K. H. J. Buschow and R. P. van Staple, *J. Appl. Phys.* **41**, 4066 (1970).
- ⁸⁸ M. Uhlarz, C. Pfleiderer, and S. M. Hayden, *Phys. Rev. Lett.* **93**, 256404 (2004).
- ⁸⁹ E. A. Yelland, S. J. C. Yates, O. Taylor, A. Griffiths, S. M. Hayden, and A. Carrington, *Phys. Rev. B* **72**, 184436 (2005).
- ⁹⁰ F. R. de Boer, C. J. Schinkel, J. Biesterbos, and S. Proost, *J. Appl. Phys.* **40**, 1049 (1969).
- ⁹¹ I. I. Mazin and D. J. Singh, *Phys. Rev. B* **69**, 020402(R) (2004).
- ⁹² A. Aguayo, I. I. Mazin, and D. J. Singh, *Phys. Rev. Lett.* **92**, 147201 (2004).
- ⁹³ L. Ortenzi, I. I. Mazin, P. Blaha, and L. Boeri, *Phys. Rev. B* **86**, 064437 (2012).
- ⁹⁴ P. Kovács, F. Tran, P. Blaha, and G. K. H. Madsen, *J. Chem. Phys.* **150**, 164119 (2019).
- ⁹⁵ J. H. Yang, D. A. Kitchaev, and G. Ceder, *Phys. Rev. B* **100**, 035132 (2019).
- ⁹⁶ J. Paier, M. Marsman, K. Hummer, G. Kresse, I. C. Gerber, and J. G. Ángyán, *J. Chem. Phys.* **124**, 154709 (2006), **125**, 249901 (2006).
- ⁹⁷ Y.-R. Jang and B. D. Yu, *J. Magn.* **16**, 201 (2011).
- ⁹⁸ Y.-R. Jang and B. D. Yu, *J. Phys. Soc. Jpn.* **81**, 114715 (2012).
- ⁹⁹ P. Janthon, S. Luo, S. M. Kozlov, F. Viñes, J. Limtrakul, D. G. Truhlar, and F. Illas, *J. Chem. Theory Comput.* **10**, 3832 (2014).
- ¹⁰⁰ W. Gao, T. A. Abtew, T. Cai, Y.-Y. Sun, S. Zhang, and P. Zhang, *Solid State Commun.* **234-235**, 10 (2016).
- ¹⁰¹ F. Tran, S. Ehsan, and P. Blaha, *Phys. Rev. Materials* **2**, 023802 (2018).
- ¹⁰² S. Jana, A. Patra, L. A. Constantin, and P. Samal, *J. Chem. Phys.* **152**, 044111 (2020).
- ¹⁰³ J. Heyd, G. E. Scuseria, and M. Ernzerhof, *J. Chem. Phys.* **118**, 8207 (2003), **124**, 219906 (2006).
- ¹⁰⁴ A. V. Krugau, O. A. Vydrov, A. F. Izmaylov, and G. E. Scuseria, *J. Chem. Phys.* **125**, 224106 (2006).
- ¹⁰⁵ M. Kuisma, J. Ojanen, J. Enkovaara, and T. T. Rantala, *Phys. Rev. B* **82**, 115106 (2010).
- ¹⁰⁶ A. Karolewski, R. Armiento, and S. Kümmel, *J. Chem. Theory Comput.* **5**, 712 (2009).
- ¹⁰⁷ A. P. Gaiduk and V. N. Staroverov, *J. Chem. Phys.* **131**, 044107 (2009).
- ¹⁰⁸ A. Svane and O. Gunnarsson, *Phys. Rev. Lett.* **65**, 1148 (1990).
- ¹⁰⁹ F. Tran, P. Blaha, K. Schwarz, and P. Novák, *Phys. Rev. B* **74**, 155108 (2006).
- ¹¹⁰ R. J. Radwanski and Z. Ropka, *Physica B* **403**, 1453 (2008).
- ¹¹¹ A. Schrön and F. Bechstedt, *J. Phys.: Condens. Matter* **25**, 486002 (2013).
- ¹¹² I. V. Solov'yev, A. I. Liechtenstein, and K. Terakura, *Phys. Rev. Lett.* **80**, 5758 (1998).
- ¹¹³ T. Shishidou and T. Jo, *J. Phys. Soc. Jpn.* **67**, 2637 (1998).
- ¹¹⁴ W. Neubeck, C. Vettier, F. de Bergevin, F. Yakhov, D. Mannix, L. Ranno, and T. Chatterji, *J. Phys. Chem. Solids* **62**, 2173 (2001).
- ¹¹⁵ W. Jauch and M. Reehuis, *Phys. Rev. B* **65**, 125111 (2002).
- ¹¹⁶ G. Ghiringhelli, L. H. Tjeng, A. Tanaka, O. Tjernberg, T. Mizokawa, J. L. de Boer, and N. B. Brookes, *Phys. Rev. B* **66**, 075101 (2002).
- ¹¹⁷ R. J. Radwanski and Z. Ropka, *Physica B* **345**, 107 (2004).
- ¹¹⁸ A. Boussendel, N. Baadji, A. Haroun, H. Dreyssé, and M. Alouani, *Phys. Rev. B* **81**, 184432 (2010).
- ¹¹⁹ V. Fernandez, C. Vettier, F. de Bergevin, C. Giles, and W. Neubeck, *Phys. Rev. B* **57**, 7870 (1998).
- ¹²⁰ A. K. Cheetham and D. A. O. Hope, *Phys. Rev. B* **27**, 6964 (1983).
- ¹²¹ W. L. Roth, *Phys. Rev.* **110**, 1333 (1958).
- ¹²² P. D. Battle and A. K. Cheetham, *J. Phys. C: Solid State Phys.* **12**, 337 (1979).
- ¹²³ H. Fjellvåg, F. Grønvald, S. Stølen, and B. Hauback, *J. Solid State Chem.* **124**, 52 (1996).
- ¹²⁴ D. C. Khan and R. A. Erickson, *Phys. Rev. B* **1**, 2243 (1970).
- ¹²⁵ D. Herrmann-Ronzau, P. Burlet, and J. Rossat-Mignod, *J. Phys. C: Solid State Phys.* **11**, 2123 (1978).
- ¹²⁶ W. Jauch, M. Reehuis, H. J. Bleif, F. Kubanek, and P. Pattison, *Phys. Rev. B* **64**, 052102 (2001).
- ¹²⁷ W. Neubeck, C. Vettier, V. Fernandez, F. de Bergevin, and C. Giles, *J. Appl. Phys.* **85**, 4847 (1999).
- ¹²⁸ J. B. Forsyth, P. J. Brown, and B. M. Wanklyn, *J. Phys. C: Solid State Phys.* **21**, 2917 (1988).
- ¹²⁹ N. O. Golosova, D. P. Kozlenko, S. E. Kichanov, E. V. Lukin, H.-P. Liermann, K. V. Glazyrin, and B. N. Savenko, *J. Alloys Compd.* **722**, 593 (2017).
- ¹³⁰ P. J. Brown, J. B. Forsyth, E. Lelièvre-Berna, and F. Tasset, *J. Phys.: Condens. Matter* **14**, 1957 (2002).
- ¹³¹ L. M. Corliss, J. M. Hastings, R. Nathans, and G. Shirane, *J. Appl. Phys.* **36**, 1099 (1965).
- ¹³² V. Baron, J. Gutzmer, H. Rundlöf, and R. Tellgren, *Solid State Sci.* **7**, 753 (2005).
- ¹³³ A. H. Hill, F. Jiao, P. G. Bruce, A. Harrison, W. Kockelmann, and C. Ritter, *Chem. Mater.* **20**, 4891 (2008).
- ¹³⁴ W. J. Takei, D. E. Cox, and G. Shirane, *Phys. Rev.* **129**,

- 2008 (1963).
- ¹³⁵ H. Holseth, A. Kjekshus, and A. F. Andresen, *Acta Chem. Scand.* **24**, 3309 (1970).
 - ¹³⁶ G. Kuhn, S. Mankovsky, H. Ebert, M. Regus, and W. Bensch, *Phys. Rev. B* **87**, 085113 (2013).
 - ¹³⁷ M. T. Czyżyk and G. A. Sawatzky, *Phys. Rev. B* **49**, 14211 (1994).
 - ¹³⁸ A. G. Petukhov, I. I. Mazin, L. Chioncel, and A. I. Liechtenstein, *Phys. Rev. B* **67**, 153106 (2003).
 - ¹³⁹ P. Mohn, C. Persson, P. Blaha, K. Schwarz, P. Novák, and H. Eschrig, *Phys. Rev. Lett.* **87**, 196401 (2001).
 - ¹⁴⁰ L. H. Thomas, *Proc. Cambridge Philos. Soc.* **23**, 542 (1927).
 - ¹⁴¹ E. Fermi, *Rend. Accad. Naz. Lincei* **6**, 602 (1927).
 - ¹⁴² C. F. von Weizsäcker, *Z. Phys.* **96**, 431 (1935).
 - ¹⁴³ T. Kotani, *J. Phys.: Condens. Matter* **10**, 9241 (1998).
 - ¹⁴⁴ I. Schnell, G. Czycholl, and R. C. Albers, *Phys. Rev. B* **68**, 245102 (2003).
 - ¹⁴⁵ P. Jemmer and P. J. Knowles, *Phys. Rev. A* **51**, 3571 (1995).
 - ¹⁴⁶ R. Neumann and N. C. Handy, *Chem. Phys. Lett.* **266**, 16 (1997).
 - ¹⁴⁷ A. C. Cancio, C. E. Wagner, and S. A. Wood, *Int. J. Quantum Chem.* **112**, 3796 (2012).